Farming and public goods production in *Caenorhabditis elegans* populations

Shashi Thutupalli[a,b,1,2,3], Sravanti Uppaluri[c,1,2,4], George W. A. Constable[d,5], Simon A. Levin[d], Howard A. Stone[a], Corina E. Tarnita[d], and Clifford P. Brangwynne[c,2]

[a]Department of Mechanical and Aerospace Engineering, Princeton University, Princeton, NJ 08544; [b]Joseph Henry Laboratories of Physics, Princeton University, Princeton, NJ 08544; [c]Department of Chemical and Biological Engineering, Princeton University, Princeton, NJ 08544; and [d]Department of Ecology and Evolutionary Biology, Princeton University, Princeton, NJ 08544

Edited by Andrea Rinaldo, Laboratory of Ecohydrology, Ecole Polytechnique Federale Lausanne, Lausanne, Switzerland, and approved January 10, 2017 (received for review June 3, 2016)

The ecological and evolutionary dynamics of populations are shaped by the strategies they use to produce and use resources. However, our understanding of the interplay between the genetic, behavioral, and environmental factors driving these strategies is limited. Here, we report on a *Caenorhabditis elegans*–*Escherichia coli* (worm–bacteria) experimental system in which the worm-foraging behavior leads to a redistribution of the bacterial food source, resulting in a growth advantage for both organisms, similar to that achieved via farming. We show experimentally and theoretically that the increased resource growth represents a public good that can benefit all other consumers, regardless of whether or not they are producers. Mutant worms that cannot farm bacteria benefit from farming by other worms in direct proportion to the fraction of farmers in the worm population. The farming behavior can therefore be exploited if it is associated with either energetic or survival costs. However, when the individuals compete for resources with their own type, these costs can result in an increased population density. Altogether, our findings reveal a previously unrecognized mechanism of public good production resulting from the foraging behavior of *C. elegans*, which has important population-level consequences. This powerful system may provide broad insight into exploration–exploitation tradeoffs, the resultant ecoevolutionary dynamics, and the underlying genetic and neurobehavioral driving forces of multispecies interactions.

foraging behavior | public goods | predator–prey | population dynamics | farming

The fitness of an organism is affected by its strategies to produce, explore, and exploit resources (1, 2). These strategies are influenced, in large part, by interdependencies among organisms, such as competition, predation (3, 4), mutualism (5–7), or the production of public good resources (8–10). Despite the wide prevalence of such interactions in nature as well as numerous theoretical and empirical studies, we are still limited in our mechanistic understanding of the interplay between different survival strategies, the resultant evolutionary dynamics and the underlying genetic, neurobehavioral, and ecological driving forces. In this pursuit, model systems in the laboratory have served as a useful bridge between the complexity of nature and the simplifications inherent in theoretical investigations. Such model systems have predominantly been either microbial (11, 12) or higher organisms, such as primates and humans (13–16). Microbial systems are very convenient due to their genetic tractability and short generation times but are limited in the space of behavioral traits they exhibit. At the other extreme, higher organisms exhibit rich neurobehavioral and genetic traits, but they are difficult to experimentally manipulate and generation times are very long.

Recently, organisms such as the nematode worm *Caenorhabditis elegans* and the fruit fly *Drosophila melanogaster* have been increasingly used in evolutionary and behavioral studies (17–19). These organisms demonstrate complex behavior and yet retain experimental tractability due to their extensive development as model systems in neurobiology and genetics. The *C. elegans* worms, in particular, are amenable to experimental tracking of large populations and multiple generations at high resolution (20–23), which has made them one of the most widely used model organisms in behavioral, genetic, and neurobiological studies.

The ecological and evolutionary backgrounds of *C. elegans*, however, have remained unclear for a long time, and only recently have insights into the organism's natural habitat begun to be uncovered. Contrary to the common perception that it is a soil nematode, *C. elegans* is primarily a colonizer of microbe-rich habitats including decaying organic matter where resources are finite and are quickly depleted (24, 25). *C. elegans* populations are characterized by a rich set of ecological dynamics: (*i*) a boom and bust population dynamics due to ephemeral resources (26), self-fertilization (27), and dauer developmental stages (28); (*ii*) dispersal and migration by various means (26); (*iii*) competition (26, 29, 30); and even (*iv*) host–microbe interactions (24, 25, 30, 31). Such a lifestyle is naturally tied with the

Significance

The population dynamics of species arise from individual-level inter- and intraspecies interactions, driven by genetic and neurobehavioral factors. However, linking ecological and evolutionary dynamics to underlying mechanisms represents a major challenge, largely due to experimental intractability. Here, we study the population dynamics of a predator–prey system comprising the nematode worm *Caenorhabditis elegans* and bacteria *Escherichia coli*. We find that the worms engage in a form of primitive agriculture, driven by their foraging behavior, by redistributing their bacterial food source, which subsequently grows. Our findings have ecoevolutionary consequences that are broadly applicable not only to worm–bacterial dynamics but also for diverse situations such as the spread of epidemics, foraging behavior, seed dispersal, and the organisms' engineering of their habitat.

Author contributions: S.T. and S.U. designed research; S.T. and S.U. performed research; S.T., S.U., G.W.A.C., S.A.L., H.A.S., C.E.T., and C.P.B. contributed new reagents/analytic tools; S.T., S.U., G.W.A.C., and C.E.T. analyzed data; and S.T., S.U., G.W.A.C., S.A.L., H.A.S., C.E.T., and C.P.B. wrote the paper.

The authors declare no conflict of interest.

This article is a PNAS Direct Submission.

[1]S.T. and S.U. contributed equally to this work.

[2]To whom correspondence may be addressed. Email: shashi@ncbs.res.in, sravanti.uppaluri@apu.edu.in, or cbrangwy@princeton.edu.

[3]Present address: Simons Centre for the Study of Living Machines, National Centre for Biological Sciences, Tata Institute for Fundamental Research, Bangalore 560065, India.

[4]Present address: School of Liberal Studies, Azim Premji University, Bangalore 560100, India.

[5]Present address: Department of Evolutionary Biology and Environmental Studies, University of Zürich, 8057 Zurich, Switzerland.

This article contains supporting information online at www.pnas.org/lookup/suppl/doi:10.1073/pnas.1608961114/-/DCSupplemental.

movement patterns of the worms through the complex environments where they dwell. In the laboratory, the foraging strategies of *C. elegans*, which are a key determinant of their fitness, are influenced both by the distribution and quality of resources (32) and by the presence of competitors (33), whether they are of the same or different genotypes, a scenario that likely results from local genetic diversity induced by worm movement (25). Therefore, *C. elegans* is an ideal model organism to study the interplay between ecology (resource distribution, inter and intraspecies interactions) and behavior (e.g., foraging strategies, public goods production) and to explore the genetic and neural circuits responsible for integrating ecological information. However, the potential for exploring these areas using *C. elegans* populations remains largely untapped.

Here, we use the *C. elegans*–bacteria (*E. coli*) system to study the emergent population dynamics of each species. *C. elegans* feed on bacteria and persistently forage for new bacterial food sources. Using both experimental and theoretical approaches, we uncover a relationship between foraging and a hitherto unrecognized mechanism of public goods production. This production of public goods leads to a long-term fitness advantage for both the worms and the bacteria, but one that can easily be exploited by nonproducing types.

Results and Discussion

Our experimental setup comprises a homogeneous surface containing nutrients for bacterial (*E. coli*) growth; *C. elegans* can dwell and feed on the growing bacteria or they can forage about the surface by crawling, their predominant form of motility. At the start of an experiment, an individual N2 (laboratory "wild type") worm is placed near a circular patch of bacteria growing at the center of a nutrient agar-filled Petri dish. As the experiment progresses, new bacterial colonies appear, both as discrete new patches or as continuous trails leading away from the initial patch (Fig. 1*A*). Because the bacterial strain we use is nonmotile, the worm's movement within and outside of the initial patch of bacteria (34, 35) is responsible for redistributing the bacterial resource.

In our experiment, the entire homogeneous agar surface is available for the worms to explore. Worms that have been feeding on fluorescent bacteria reveal two mechanisms for the formation of new bacterial colonies. Bacterial food is propelled through the worm digestive system, and undigested material is excreted (36). Thus, while locomoting, worms may defecate undigested bacteria as illustrated in Fig. 1*B* (also see Movie S1), which can eventually grow into larger bacterial colonies. A second and much more prevalent source of bacterial dispersal arises from adhesion of the bacteria to the surface of the worm body. When the worm moves out of a dense bacterial colony, some bacteria hitchhike on the worm's surface and are sloughed off through fluid entrainment as the worm crawls around its arena (Fig. 1*C*; also see Movie S2); these bacteria then also grow into colonies. Redistributed colonies represent a new food resource, which can be revisited and used by the worms (Fig. 1*D*). The dynamics are not unique to flat Petri-dish surfaces but also occur in native environments such as rotting fruit (Fig. 1*E*) and 3D porous soil (Fig. 1*F*).

Farming of Bacteria by the *C. elegans* Worms. The bacterial redistribution has consequences for the population dynamics of both

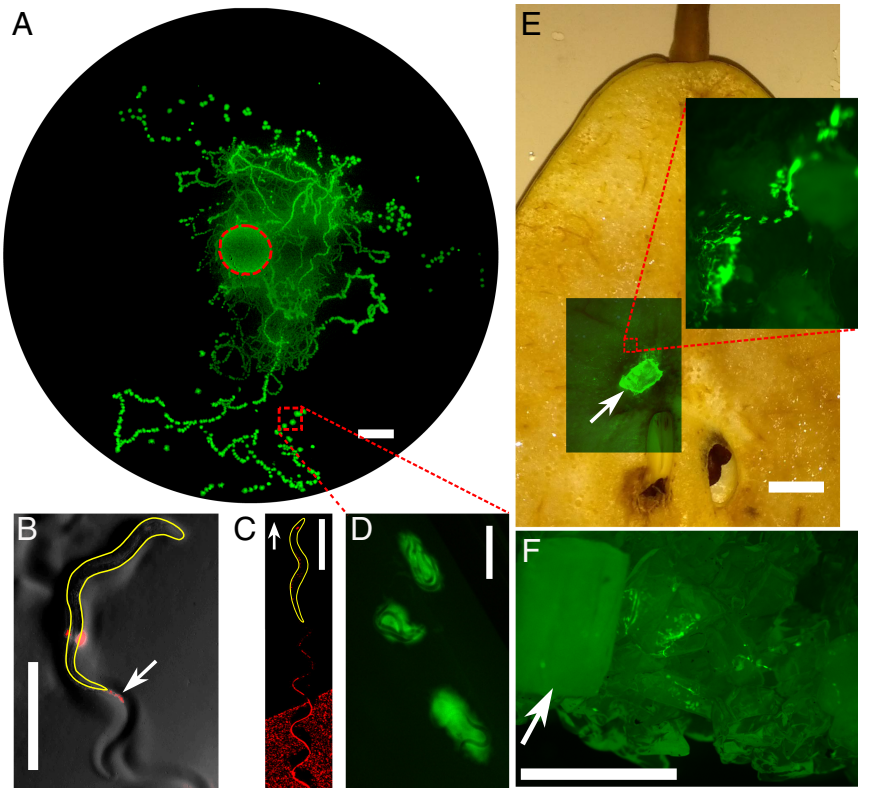

Fig. 1. Redistribution and growth of *E. coli* bacteria due to locomotion of *C. elegans*. (*A*) Trails and patches of bacteria are found away from an initial circular patch (red dashed circle) of bacterial inoculation in which a single worm is placed. The image is taken 4 d after seeding of a bacterial patch with a worm. The bacterial redistribution is due to two main mechanisms: defecation of ingested bacteria (white arrow points to red "feces") by the worm (*B*) and entrainment of the bacteria (red) in the wake of the locomoting worm (white arrow shows direction of motion) (*C*). (*D*) Worms revisit and colonize the redistributed, growing bacterial patches. Worms disperse bacteria in natural settings such as rotting fruit (*E*) and soil-like porous medium (*F*). Arrows indicate initial chunk of worms and bacteria. (Scale bars: *A*, *E*, and *F*, 1 cm; *B*–*D*, 500 μm.)

bacteria and worms, which we explore via experiments and mathematical modeling. We first sought to examine how the population dynamics are impacted when we limit the ability of the worms to redistribute bacteria. We take advantage of the genetic tractability of this system by using worms with a mutation in the srf-3 gene, which causes altered body surface properties that reduce surface adhesion by bacteria (37, 38). The exploratory behavior of *srf-3* mutants is comparable to that of the N2 worms (*SI Appendix*, Fig. S1), but they do not cause significant bacterial dispersal (Fig. 2*A*). By dispersing bacteria from a single large patch into several smaller patches, N2 worms decrease the density of the bacterial colonies. Smaller, less dense patches of bacteria grow faster than large, denser patches due to an increased availability of local nutrients on the agar surface (*SI Appendix*, Fig. S2). Thus, bacterial dispersal by N2 worms, but not by the *srf-3* mutant, results in an increase in the overall population growth rate of the bacteria (Fig. 2*B*). This difference in their ability to disperse their bacterial resource has a significant impact on worm population dynamics; under identical initial conditions, the N2 population grew larger than that of the *srf-3* worms (Fig. 2*C*; brood sizes of both worm types are comparable as shown in *SI Appendix*, Fig. S3).

This behavior appears to reflect a type of "bacterial farming," whereby the consumer (worm) benefits from increasing its food resource (bacteria) by facilitating the bacteria's access to a third resource, the agar nutrients. To test this idea, we asked whether increasing the Petri dish size—and thus increasing the local availability of agar nutrients—would increase worm proliferation. Keeping the size of the initial bacterial seed colony constant and with saturated concentrations of bacterial nutrients in the agar (*SI Appendix*, Fig. S4), increasing dish size up to a critical radius of 7.5 cm had little effect on the *srf-3* population, while having a dramatic positive effect—more than twofold increase with the available exploration area—on the N2 population (Fig. 3). This difference between N2 and *srf-3* worms occurs despite the fact that both worm types engage in similar space exploration strategies (*SI Appendix*, Fig. S1). Moreover, upon artificial dispersal of bacteria into multiple patches, both worms are found to exhibit a similar up-regulation of their reproduction in response to the increased food availability (Fig. 3*A*, *Inset*). These results suggest that the N2 behavior seen in Fig. 3 does indeed represent a type of farming. Beyond the critical plate size, although N2 populations remained larger than *srf-3* ones, both *srf-3* and N2 population sizes decreased with plate size, which may reflect a decreased birth rate associated with long-distance exploration.

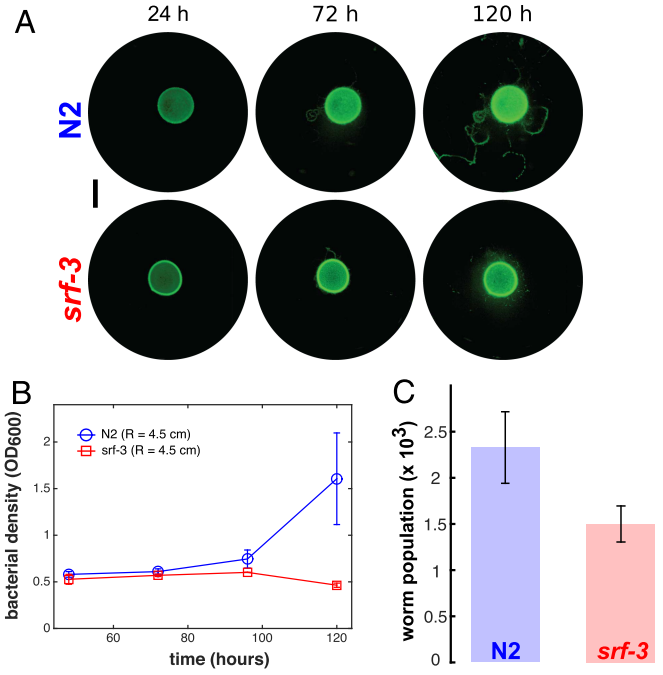

Fig. 2. Farming confers a population growth advantage. (*A*) N2 worms redistribute bacteria, whereas *srf-3* mutants do not. (Scale bar: 1 cm.) (*B*) Bacterial density on plates (R = 4.5 cm) with N2 (blue circles, n = 4) and *srf-3* (red squares, n = 4). (*C*) The population sizes of N2 worms and the mutant type *srf-3* worms 144 h after the start of the experiment for the same initial conditions.

Mathematical Model. To understand the farming behavior, we constructed a theoretical model that allowed us to test the proposed farming mechanism but also to explore further scenarios of interest and make testable predictions. To retain the simplicity and versatility of the model, we sacrificed complex and little-understood details related to spatial movement, such as the use of memory, and instead captured the relevant qualitative behavior implicitly via physically and experimentally motivated assumptions. The model consists of age-structured, spatially implicit ordinary differential equations that capture the population dynamics of the worms and the impact of their foraging behaviors on bacterial dynamics (the text in *SI Appendix* and *SI Appendix*, Figs. S5–S9). Because the feeding and farming behaviors of the worms affect the area and density of bacteria in ways that cannot be captured by the total number of bacteria alone, we characterize the bacteria via their spatial distribution (captured by area, A_B) and via their density ρ, assumed to be homogeneous but time-dependent. In the absence of worms, both area and density grow logistically. The worm population is age-structured into four stages: eggs, sexually immature, mature, and infertile worms. Eggs hatch at a fixed rate to become immature worms, which then progress through the three stages of their adult life cycle at a rate proportional to the amount of bacteria consumed. As the bacteria get depleted, their density decreases, whereas their area is preserved, an assumption supported visually by experiments (Fig. 2*A*). Worms feed according to a Holling's type II form, $F(A_B, \rho, R)$, featuring an encounter rate between worms and bacteria. To capture this behavior in a spatially implicit way we let the encounter rate, $\psi(A_B, R)$, be a function of bacterial area and plate radius, R: the more bacteria relative to the size of the plate, the higher the encounter rate:

$$F(A_B, \rho, R) = \frac{c\psi(A_B, R)\rho A_B}{1 + c\psi(A_B, R)\rho A_B}, \quad [1]$$

$$\psi(A_B, R) = \exp\left(\frac{-\pi R^2}{\sigma A_B}\right). \quad [2]$$

The parameter c controls how quickly the feeding rate increases in response to increased bacteria, whereas the parameter σ controls how quickly the encounter rate declines with plate size. In reality, the encounter rate between worms and bacteria depends on a range of *C. elegans* characteristics, including their exploration–exploitation strategies, foraging behavior, and memory. In our simplified model, we propose the phenomenological form above for $\psi(A_B, R)$ to capture the experimental observation that the mean feeding/reproductive rate decreases with large plate sizes (Fig. 3).

Farmers increase the spatial distribution of the bacteria, thus simultaneously decreasing its density. The rate of bacterial spreading is proportional to the amount of free space on the plate, the density of the bacteria, and the encounter rate:

$$S(B, R) = s\psi(A_B, R)\rho(\pi R^2 - A_B). \quad [3]$$

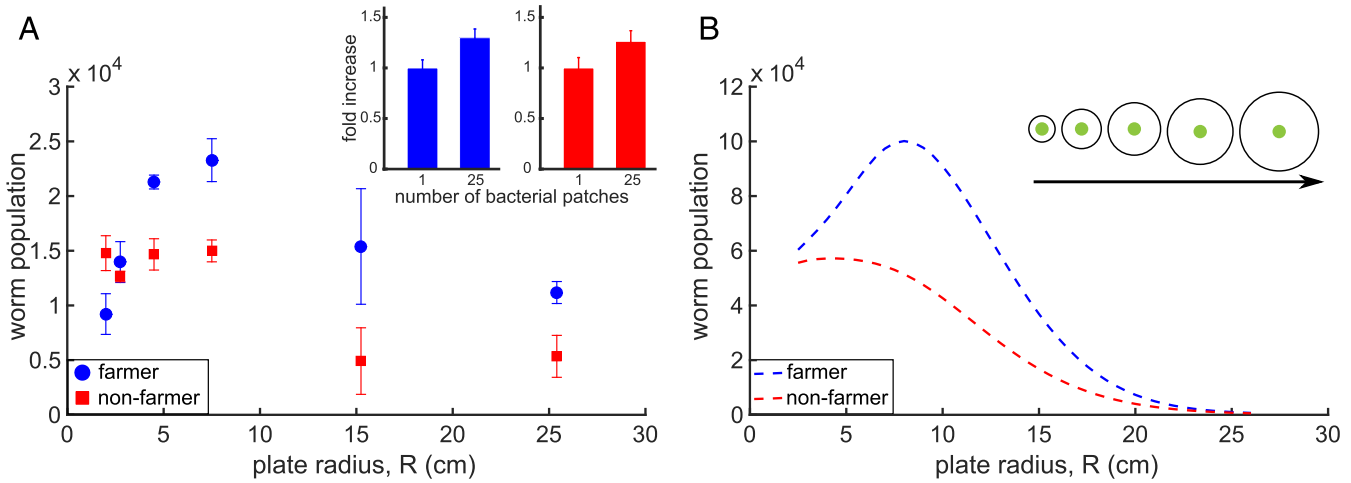

Fig. 3. Effect of available farming area on the worm population. Worm population as a function of the available dispersal area for the farmer (N2, blue) and nonfarmer (*srf-3* mutant, red) worms. (*A*) Experiments. (*B*) Numerical results. (*A*, *Inset*) Experiments indicating the fold increase in population size of the worms grown on artificially distributed bacterial patches. The data are normalized to a onefold increase in the case of one bacterial patch. Measurements were made 72 h after initialization. The initial amount of bacteria is the same but the patches are distributed either as 1 large patch or the 25 smaller patches formed in a 5 × 5 grid; n = 2–5 for each plate size. (*B*, *Inset*) Schematic of the experiment. The bacterial patch is kept constant, whereas the dish size is increased.

Nonfarmers do not spread bacteria and, hence, $s = 0$. We are able to derive experimentally the majority of our parameters (the text in *SI Appendix* and *SI Appendix*, Table S1). The only free parameters pertain to the worm spatial feeding behavior (c and σ) and, in the case of the farmer, the spreading behavior, s. Despite its simplicity and low-dimensionality, our model robustly recapitulates qualitatively (with fourfold quantitative difference) the complex population dynamics of the worms and bacteria (Fig. 3, *SI Appendix*, Figs. S5–S6, and Movies S3 and S4). A further simplified version of this model that ignores the age structure of the worm population also recapitulates the dynamics qualitatively, showing the robustness of our physically motivated assumptions, but does so at the expense of having more free parameters and a worse quantitative fit (see *SI Appendix* and Movie S5 for details).

Redistributed Bacteria Is a Potentially Costly Public Good. Despite the inability of *srf-3* worms to farm, if a mixed population includes N2 worms that farm and therefore increase the bacterial resource, all worms may be able to take advantage of it. To experimentally test this hypothesis, we competed mixed populations containing both worm types, starting with varying initial ratios of farmer (N2) to nonfarmer (*srf-3*). We found that both phenotypes equally share the farming-increased resource, and the benefits scale linearly with the proportion of farmers (Fig. 4*A*). This result shows that the farming of bacteria by N2 worms is a public good and that on agar plates there is no significant spatial clustering that would cause the public good to be mostly shared with kin. Given the small difference in the benefit gained by the farming and nonfarming populations, this public good appears to be generated with negligible additional metabolic cost to the farmers.

Although we are unable to detect significant fitness costs incurred by N2 farmers compared with the *srf-3* nonfarmers, costs associated with public goods production are likely to occur in nature and can strongly impact the evolutionary dynamics of mixed populations of producers and nonproducers. In our system, there are at least two ways in which costs may arise. First, although prolonged exposure to *E. coli* does not appear to be harmful for the worms, other types of bacteria commonly found in nature are highly pathogenic to the worm (37, 38). Consequently, bacterial entrainment arising from worm stickiness could increase this pathogenicity, whereas the nonstickiness of the *srf-3* worms could confer resistance to pathogenic bacteria (37, 38). Second, metabolic costs associated with foraging are known to occur and mutants adopting different foraging strategies will necessarily incur different costs.

We use our mathematical model to explore the public good production and the effects of possible costs on the worm population dynamics. If there is no cost to farming, farmers and nonfarmers perform equally well in mixed cultures, consistent with our experimental findings (Fig. 4 *A*–*C*). However, we find significant difference in performance in two competition scenarios: between farmers and nonfarmers when the farmers pay an increased mortality cost due to bacterial pathogenicity (scenario 1) and between two farmers with different foraging behaviors (scenario 2); a more efficient forager that can find bacteria quickly but at a higher cost to its reproduction and a slower forager that incurs a lower reproductive cost. As expected, in scenario 1, we find that farmers that pay a mortality cost are worse off, whereas nonfarmers are better off (Fig. 4*D* and *SI Appendix*, Fig. S10). In scenario 2, depending on the magnitude of the cost, better-foraging farmers can perform worse in competition with the poorer foragers (*SI Appendix*, Figs. S11 and S12). These outcomes may change however in a spatially structured environment where worm movement is limited (e.g., soil), and the public good is mainly available to related individuals (6, 39). Interestingly, we found that when the composition of the population is homogeneous (i.e., comprising only a single phenotype), farmers that pay a cost either to mortality (Fig. 4*E*) or to reproduction (*SI Appendix*, Figs. S10 and S12) reach higher population densities than farmers that pay lower or no cost. This counterintuitive result stems from the fact that increased worm mortality or lowered worm reproduction can reduce the pressure on the bacterial resource and in turn lead to higher worm growth in the long term. Thus, although a cost makes farmers vulnerable to exploitation in mixed cultures, it leads to higher population densities if interactions are clonal, which reinforces the importance of spatially structured environments with limited dispersal in shaping *C. elegans* behavior.

Conclusions

We have shown that *C. elegans* worms engage in a primitive form of farming of the bacterial resource that they feed on. The farming is brought about by the redistribution of bacteria

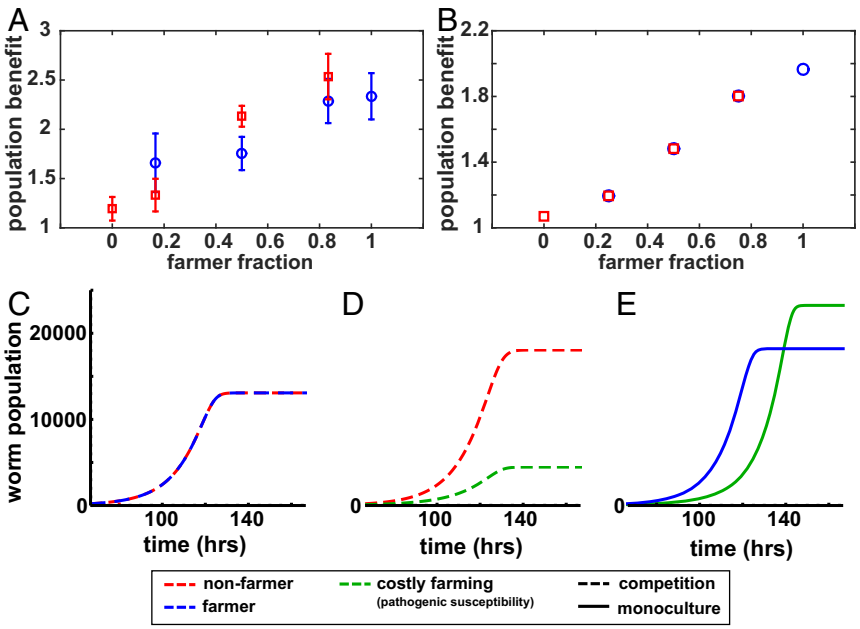

Fig. 4. Redistributed bacteria is a potentially costly public good. (*A*) Normalized worm population from competition experiments between N2 worms and *srf-3* mutant for two different plate sizes (R = 7.5 cm and R = 2.75 cm). The population increase is the ratio of the worm population on the R = 7.5 cm plate to the population on the R = 2.75 cm plate. n = 4 for each experiment. (*B*) Corresponding data of the competition between farmers and nonfarmers from mathematical model (see *SI Appendix* for details). (*C*–*E*) Mathematical model trajectories of worm population sizes in competitive (solid curves) or clonal (dashed curves) growth conditions. Worm counts are normalized by the initial numbers of that phenotype in the simulation. Competitive dynamics of farmers and nonfarmers (red) when farming inflicts no mortality cost (blue) (*C*) and some mortality cost (green) (*D*). (*E*) Clonal dynamics of farmers with and without mortality cost. The plate size is R = 7.5 cm. All parameters are as in *SI Appendix*, Table S1.

by foraging worms, resulting in an increased amount of bacteria, which can be exploited by nonproducers. This form of public goods production, which may be incidental to the foraging behavior of the worms, is qualitatively different from situations in which the good production is associated only with the explicit metabolic cost of chemical synthesis of the good, a mechanism often at play in microbial systems (6, 8–10), which lack complex behaviors. In contrast, the mechanism of public goods production that we describe here could be associated with neurobehavioral traits, such as exploration–exploitation strategies (18, 19, 29, 40–42) or the use of spatial memory (42, 43), in addition to potential metabolic costs associated with carrying the bacteria (37, 38). Moreover, *C. elegans* also appear to be capable of dispersing *Dictyostelium discoideum* spores (44), another food source; given that *D. discoideum* themselves farm bacteria (7), we anticipate a rich set of multitrophic level dynamics and niche partitioning to emerge in multispecies interactions involving the kind of effects that we have uncovered here. More specifically, these previously unobserved effects of worm-foraging behavior are likely to have significant consequences for experimental work involving *C. elegans* populations; even the most routine aspects of worm maintenance in the laboratory are likely to be affected by these dynamics.

The dynamics in our system have a striking similarity to a range of spreading processes in nature such as the dispersal of seeds or the carrying of commensal infectious agents by mobile vectors (14, 45, 46). Empirical data in these cases are limited, and even when available, the data are observational rather than experimental. Moreover, in processes such as the dispersal of seeds (46), the benefit to the disperser likely occurs on a much longer time scale compared with the benefit accrued by the dispersed. In contrast, the impact of the bacterial redistribution reported here occurs on a fast time scale, with effects similar to those of farming in other organisms (7, 47–51). This characteristic allows for experimental and theoretical investigations into the role of farming in driving and shaping the evolutionary dynamics of foraging. In addition, the microbial populations on which the worms feed are redistributed through the ecological landscape, which affects the composition of microbial communities and their relationships and interactions. Altogether, these effects will shape the local microbial and worm ecologies in ways that significantly affect their dynamics. Although further investigations are needed to determine the impact of such dynamics in the wild, this incidental dropping of "resource seeds" is remarkably similar to the early stages of human agriculture during which "... people who gathered [wheat] grains carried them back to their temporary campsites for processing...some of them inevitably fell on the way to the campsite and were lost. Over time, more and more wheat grew along favorite human trails and near campsites" (52).

Materials and Methods

***C. elegans* Strains and Culture.** N2 Bristol (laboratory wild type) and AT10 (*srf-3* (yj10)) (mutant type) were obtained from the Caenorhabditis Genetics Center (CGC) and maintained on standard nematode growth medium (NGM) plates supplemented with ampicillin and seeded with OP50-GFP *E. coli* (GFP plasmid pFVP25.1 with ampicillin resistance) also obtained from the CGC. For competition experiments, CPB089 (Pdao5:dao5:GFP), with the same brood size as N2 worms, generated in house by CRISPR technology, was used as a substitute. For all experiments, 20 μL of bacteria at $OD_{600} = 2.0$ per worm were seeded on NGM plates of the appropriate size. Worms were age-synchronized by bleaching and individual larval stage 4 (L4) worms were placed onto dishes of the appropriate size. Brood size was quantified by counting the number of embryos laid in 24-h intervals by age-synchronized worms on standard NGM plates, at which time worms were moved to a fresh dish. OD_{600} shown in Fig. 2 was measured using a NanoDrop (ThermoScientific) by washing each plate with the same volume of M9 buffer.

Imaging. To image entire Petri dish surfaces such as in Fig. 1*A*, we used a desktop flatbed scanner (Epson V700) custom-fitted with a blue light LED

strip to excite fluorescence emission in the OP50-GFP *E. coli* and a corresponding photographic emission filter (Kodak) to record the image.

Flow Cytometry. Individual plates were carefully washed with M9 buffer and inspected to collect all worms. Worm samples were washed to remove bacteria and then transferred to a Complex Object Parametric Analyzer and Sorter Biosort (Union Biometrica) sample cup at a dilution of approximately one nematode per microliter in M9 buffer. To distinguish N2 and mutant worms, fluorescent gates were determined by running fluorescent worms and nonfluorescent worms separately. All data are shown as means F0B1 SEM.

ACKNOWLEDGMENTS. We thank Christina DeCoste (Princeton Flow Cytometry Resource Facility) for invaluable assistance with the COPAS Biosort. We are grateful to Paulina Orillac for help with the initial setup of the experiments. We thank Mochi Liu for help with worm tracking and Bindu Madhav U for help with worm counting. Worm and bacterial strains were obtained from the CGC, which is funded by NIH Office of Research Infrastructure Programs Grant P40 OD010440. S.T. acknowledges the Human Frontier Science Program (Cross Disciplinary Fellowship) for funding. C.P.B. and S.U. acknowledge support from NIH Director's New Innovator Award 1DP2GM105437-01 and Searle Scholars Program Grant 12-SSP-217. S.L. was supported by Simons Foundation Grant 395890.

1. Charnov EL (1976) Optimal foraging, the marginal value theorem. *Theor Popul Biol* 9(2):129–136.
2. MacArthur RH (1972) Geographical Ecology: Patterns in the Distribution of Species (Harper and Row, New York).
3. Brooks JL, Dodson SI (1965) Predation, body size, and composition of plankton. *Science* 150(3692):28–35.
4. Oksanen L (1992) Evolution of exploitation ecosystems I. Predation, foraging ecology and population dynamics in herbivores. *Evol Ecol* 6(1):15–33.
5. Grossart HP, Dziallas C, Leunert F, Tang KW (2010) Bacteria dispersal by hitchhiking on zooplankton. *Proc Natl Acad Sci USA* 107(26):11959–11964.
6. Drescher K, Nadell CD, Stone HA, Wingreen NS, Bassler BL (2014) Solutions to the public goods dilemma in bacterial biofilms. *Curr Biol* 24(1):50–55.
7. Brock DA, Douglas TE, Queller DC, Strassmann JE (2011) Primitive agriculture in a social amoeba. *Nature* 469(7330):393–396.
8. Velicer GJ, Kroos L, Lenski RE (2000) Developmental cheating in the social bacterium *Myxococcus xanthus*. *Nature* 404(6778):598–601.
9. Griffin AS, West SA, Buckling A (2004) Cooperation and competition in pathogenic bacteria. *Nature* 430(7003):1024–1027.
10. Gore J, Youk H, van Oudenaarden A (2009) Snowdrift game dynamics and facultative cheating in yeast. *Nature* 459(7244):253–256.
11. Jessup CM, Forde SE, Bohannan BJM (2005) Microbial experimental systems in ecology. *Adv Ecol Res* 37(04):273–307.
12. Kawecki TJ, et al. (2012) Experimental evolution. *Trends Ecol Evol* 27(10):547–560.
13. Vishwanath G, da Luz M, Raposo EP, Stanley E (2011) The Physics of Foraging (Cambridge Univ Press, Cambridge, UK).
14. Brockmann D, Hufnagel L, Geisel T (2006) The scaling laws of human travel. *Nature* 439(7075):462–465.
15. Ledyard JO (1995) Public goods: A survey of experimental research. Handbook of Experimental Economics, eds Kagel J, Roth AE. (Princeton Univ Press, Princeton), pp 111–251.
16. Grujic J, Fosco C, Araujo L, Cuesta JA, Sanchez A (2010) Social experiments in the mesoscale: Humans playing a spatial prisoner's dilemma. *PLoS One* 5(11): e13749.
17. Prasad NG, Joshi A (2003) What have two decades of laboratory life-history evolution studies on *Drosophila melanogaster* taught us? *J Genet* 82(1-2):45–76.
18. Gray JC, Cutter AD (2014) Mainstreaming *Caenorhabditis elegans* in experimental evolution. *Proc Biol Sci* 281(1778):20133055.
19. Stephens GJ, Johnson-Kerner B, Bialek W, Ryu WS (2008) Dimensionality and dynamics in the behavior of *C. elegans*. *PLoS Comput Biol* 4(4):e1000028.
20. Nguyen JP, et al. (2016) Whole-brain calcium imaging with cellular resolution in freely behaving *Caenorhabditis elegans*. *Proc Natl Acad Sci USA* 113(8):E1074–E1081.
21. Venkatachalam V, et al. (2015) Pan-neuronal imaging in roaming *Caenorhabditis elegans*. *Proc Natl Acad Sci USA* 113(8):1082–1088.
22. Stroustrup N, et al. (2013) The *Caenorhabditis elegans* lifespan machine. *Nat Methods* 10(7):665–70.
23. Yemini E, Jucikas T, Grundy LJ, Brown AE, Schafer WR (2013) A database of *Caenorhabditis elegans* behavioral phenotypes. *Nat Methods* 10(9):877–879.
24. Félix MA, Braendle C (2010) The natural history of *Caenorhabditis elegans*. *Curr Biol* 20(22):R965–R969.
25. Frézal L, Félix MA (2015) *C. elegans* outside the Petri dish. *Elife* 4:1–14.
26. Félix MA, Duveau F (2012) Population dynamics and habitat sharing of natural populations of *Caenorhabditis elegans* and *C. briggsae*. *BMC Biol* 10(1):59.
27. Cutter AD (2004) Sperm-limited fecundity in nematodes: How many sperm are enough? *Evolution* 58(3):651–655.
28. Green JWM, Snoek LB, Kammenga JE, Harvey SC (2013) Genetic mapping of variation in dauer larvae development in growing populations of *Caenorhabditis elegans*. *Heredity* 111(4):306–313.
29. Gloria-Soria A, Azevedo RBR (2008) npr-1 regulates foraging and dispersal strategies in *Caenorhabditis elegans*. *Curr Biol* 18(21):1694–1699.
30. Cutter AD (2015) Caenorhabditis evolution in the wild. *Bioessays* 37(9):983–995.
31. Dirksen P, et al. (2016) The native microbiome of the nematode *Caenorhabditis elegans*: Gateway to a new host-microbiome model. *BMC Biol* 14(1):1–16.
32. Shtonda BB, Avery L (2006) Dietary choice behavior in *Caenorhabditis elegans*. *J Exp Biol* 209(Pt 1):89–102.
33. Greene JS, et al. (2016) Balancing selection shapes density-dependent foraging behaviour. *Nature* 539(7628):254–258.
34. Milward K, Emanuel K, Joseph R, Bono MD, Olofsson B (2011) Neuronal and molecular substrates for optimal foraging in *Caenorhabditis elegans*. *Proc Natl Acad Sci USA* 108(51):20672–20677.
35. Bendesky A, Tsunozaki M, Rockman MV, Kruglyak L, Bargmann CI (2011) Catecholamine receptor polymorphisms affect decision-making in *C. elegans*. *Nature* 472(7343):313–318.
36. McGhee J (2007) The *C. elegans* intestine. *WormBook* Mar 27:1–36.
37. Höflich J, et al. (2004) Loss of srf-3-encoded nucleotide sugar transporter activity in *Caenorhabditis elegans* alters surface antigenicity and prevents bacterial adherence. *J Biol Chem* 279(29):30440–30448.
38. Cipollo JF, Awad AM, Costello CE, Hirschberg CB (2004) srf-3, a mutant of Caenorhabditis elegans, resistant to bacterial infection and to biofilm binding, is deficient in glycoconjugates. *J Biol Chem* 279(51):52893–52903.
39. Nowak MA (2006) Five rules for the evolution of cooperation. *Science* 314(5805):1560–1563.
40. Croll N (1975) Behavioural analysis of nematode movement. *Adv Parasitol* 13:71–122.
41. Salvador LCM, Bartumeus F, Levin SA, Ryu WS (2014) Mechanistic analysis of the search behaviour of *Caenorhabditis elegans*. *J R Soc Interface* 11(92):20131092.
42. Calhoun AJ, Chalasani SH, Sharpee TO (2014) Maximally informative foraging by *Caenorhabditis elegans*. *Elife* 3:1–13.
43. Calhoun AJ, et al. (2015) Neural mechanisms for evaluating environmental variability in *Caenorhabditis elegans*. *Neuron* 86(2):428–441.
44. Kessin RH, Gundersen GG, Zaydfudim V, Grimson M (1996) How cellular slime molds evade nematodes. *Proc Natl Acad Sci USA* 93(10):4857–4861.
45. Hallatschek O, Fisher DS (2014) The acceleration of evolutionary spread by long-range dispersal. *Proc Natl Acad Sci USA* 111(46):E4911–E4919.
46. Howe HE, Smallwood J (2013) Ecology of seed dispersal. *Annu Rev Ecol Syst* 13(1982):201–228.
47. Rindos D (1984) The Origins of Agriculture (Academic, Orlando, FL).
48. Hata H, Kato M (2006) A novel obligate cultivation mutualism between damselfish and Polysiphonia algae. *Biol Lett* 2:593–596.
49. Mueller UG, Gerardo NM, Aanen DK, Six DL, Schultz TR (2005) The evolution of agriculture in insects. *Annu Rev Ecol Evol Syst* 36:563–595.
50. Silliman BR, Newell SY (2003) Fungal farming in a snail. *Proc Natl Acad Sci USA* 100(26):15643–15648.
51. Qiu D, Huang L, Lin S (2016) Cryptophyte farming by symbiotic ciliate host detected in situ. *Proc Natl Acad Sci USA* 113(43):12208–12213.
52. Harari YN (2014) Sapiens - A Brief History of Humankind (Harper, New York).

Supporting Information

Thutupalli et al. 10.1073/pnas.1608961114

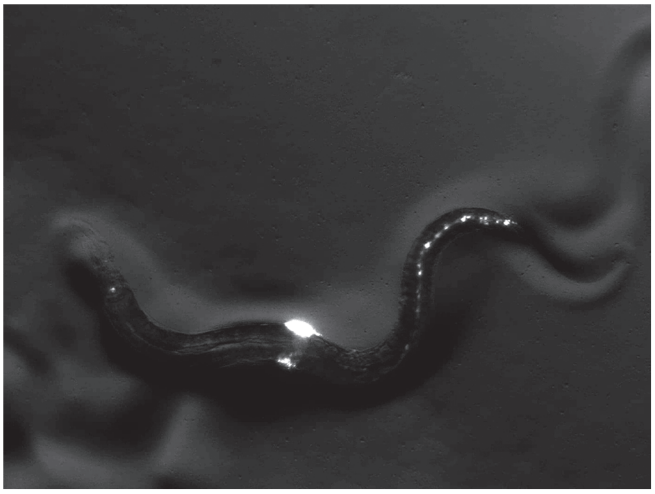

Movie S1. Defecation of fluorescently (GFP) labeled colloidal particles (1 μm in diameter) by an N2 *C. elegans* worm. The worm was transferred onto a lawn of nonfluorescent bacteria (*E. coli*, OP50) after feeding on bacteria seeded with fluorescent beads. The movie was captured at 10 frames per second (fps) and played back in real time. The length of the worm is about 1 mm.

Movie S1

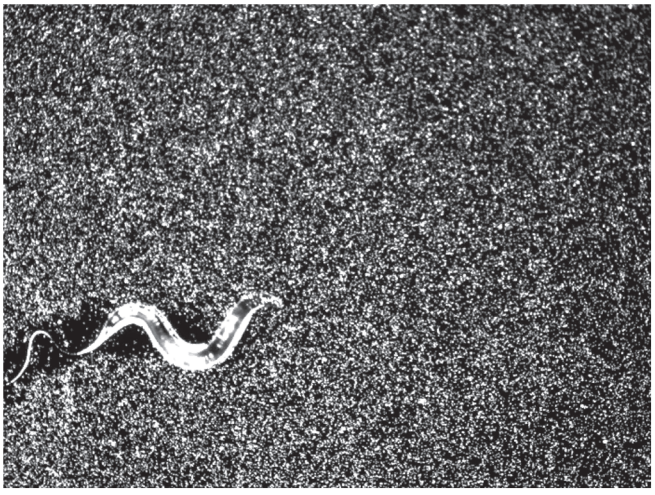

Movie S2. Entrainment of fluorescently (GFP) labeled colloidal particles (1 μm in diameter) due to the locomotion of N2 *C. elegans* worm. The movie was captured at 10 fps and played back in real time. The length of the worm is about 1 mm.

Movie S2

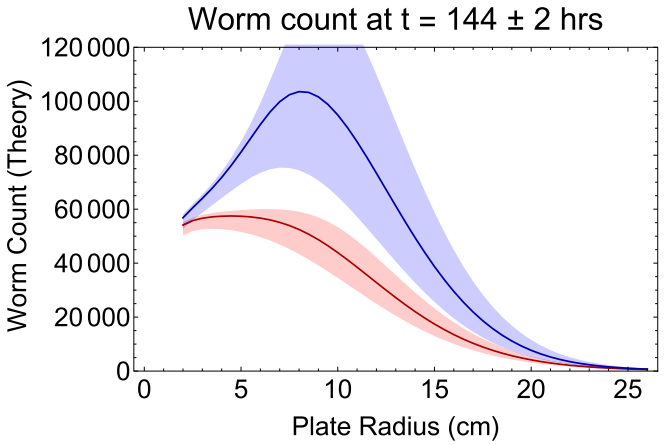

Movie S3. A graphical illustration of the sensitivity of the worm count in the age-structured spatially implicit model, discussed in *Results and Discussion* and in *SI Appendix*, *2.2 Spatially Implicit Model*, to varying the three free parameters in the model. The parameter c, the saturation rate of the Hollings type II functional response (*SI Appendix*, Eq. **S.3**), is varied over a 15-fold increase, from $c = 5 \times 10^{-10}$ to $c = 7.5 \times 10^{-9}$ cells^{-1}. The parameter σ, which controls how the worms' foraging efficiency changes with plates size (*SI Appendix*, Eq. **S.4**), is varied over a 20-fold increase, from $\sigma = 100$ to $\sigma = 2{,}000$ cm^2. The parameter s, the rate at which bacteria is spread by farmers (*SI Appendix*, Eq. **S.5**), is varied over a 300-fold increase, from $s = 7 \times 10^{-11}$ to $s = 2.1 \times 10^{-8}$ min^{-1}cm^{-2}.

Movie S3

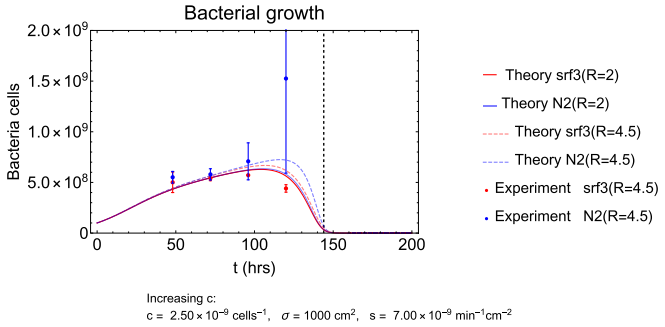

Movie S4. A graphical illustration of the sensitivity of the bacterial dynamics in the age-structured spatially implicit model, discussed in *Results and Discussion* and in *SI Appendix*, *2.2 Spatially Implicit Model*, to varying the three free parameters in the model. The experimentally measured time to collapse of the bacterial population on the $R = 2$-cm plate, $t = 144$ h, is plotted as the vertical dashed black line. The parameter c, the saturation rate of the Holling's type II functional response (*SI Appendix*, Eq. **S.3**), is varied over a 15-fold increase, from $c = 5 \times 10^{-10}$ to $c = 7.5 \times 10^{-9}$ cells^{-1}. The parameter σ, which controls how the worms' foraging efficiency changes with plate size (*SI Appendix*, Eq. **S.4**), is varied over a 20-fold increase, from $\sigma = 100$ to $\sigma = 2{,}000$ cm^2. The parameter s, the rate at which bacteria is spread by farmers (*SI Appendix*, Eq. **S.5**), is varied over a 300-fold increase, from $s = 7 \times 10^{-11}$ to $s = 2.1 \times 10^{-8}$ min^{-1}cm^{-2}.

Movie S4

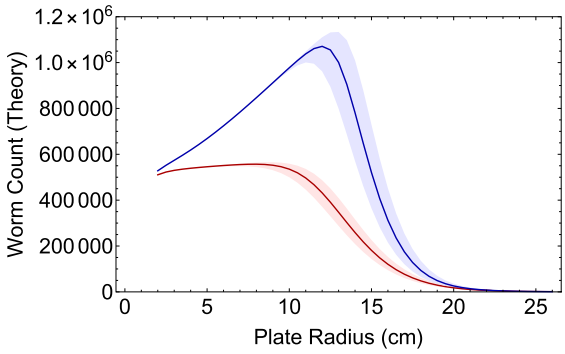

Increasing a

a = 9.00 cells min^{-1}, ϵ = 0.0045 min^{-1}, c = 1.4 × 10^{-9} cells^{-1}, σ = 1200 cm^2, s = 1. × 10^{-10} min^{-1}cm^{-2}

Movie S5. A simple spatially implicit model, featuring a single class of worm and five free parameters, is described in *SI Appendix*, *2.1 Spatially Implicit Model*. The worm count predicted by this model is taken at $t = 144$ h, the same time at which the worm count was experimentally measured. This timing corresponds to the bacterial population being driven to collapse by the *C. elegans* population on the smallest plate ($R = 2$ cm). This movie shows the sensitivity of the model's predicted worm count to varying its five free parameters. The parameter a, the maximum rate at which worms can consume bacteria, is varied over a 20-fold increase, from $a = 1$ to $a = 20$ cells/min. The parameter ϵ, the worm reproductive rate, is varied from $\epsilon = 3.5 \times 10^{-3}$ to $\epsilon = 5.5 \times 10^{-3}$ min^{-1}. The parameter c, the saturation rate of the Hollings type II functional response (*SI Appendix*, Eq. **S.3**), is varied over a fivefold increase, from $c = 5 \times 10^{-10}$ to $c = 2.5 \times 10^{-9}$ cells^{-1}. The parameter σ, which controls how the worms' foraging efficiency changes with plates size (*SI Appendix*, Eq. **S.4**), is varied over a fourfold increase, from $\sigma = 500$ to $\sigma = 2{,}000$ cm^2. The parameter s, the rate at which bacteria is spread by farmers (*SI Appendix*, Eq. **S.5**), is varied over a 15-fold increase, from $s = 1 \times 10^{-11}$ to $s = 1.5 \times 10^{-10}$ min^{-1}cm^{-2}.

Movie S5

Other Supporting Information Files

SI Appendix (PDF)

Supplementary Materials for

Farming and public goods production in *C. elegans* populations

Shashi Thutupalli, Sravanti Uppaluri, George W.A. Constable, Simon A. Levin, Howard A. Stone, Corina E. Tarnita, Clifford P. Brangwynne

correspondence to: S.T.: shashi@ncbs.res.in, S.U.: sravanti.uppaluri@apu.edu.in, C.P.B.: cbrangwy@princeton.edu

1 Supplementary Experimental Data

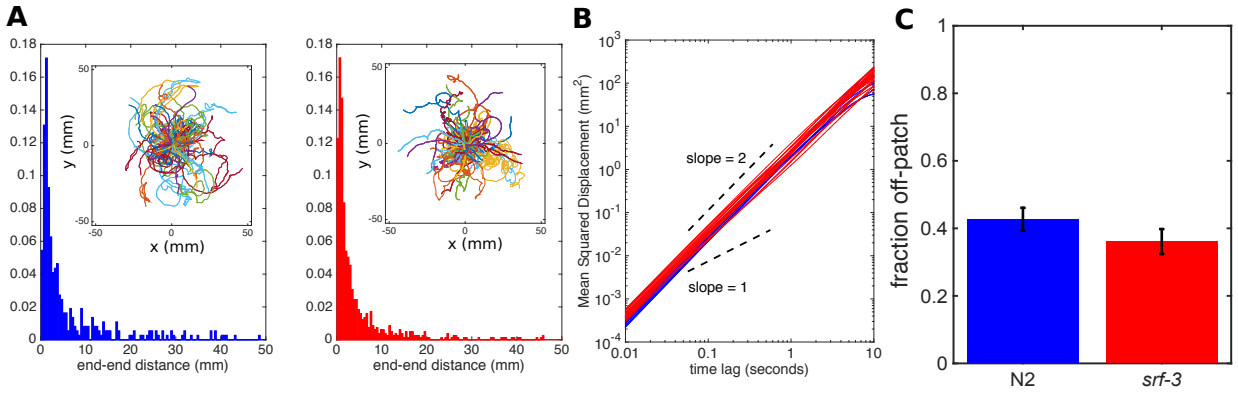

Figure S1: **A**. Trajectory analysis of farmer/wild type worms (blue data, $n = 400$ tracks) and non-farmer/*srf-3* mutant (red data, $n = 400$ tracks) showing the distribution of end-end distances of multiple trajectories obtained by tracking 10 worms on a bacteria-free agar surface of each type over a period of 4 hours. **B.** The mean squared displacements for the trajectories shown in panel **A.** Red curves represent the non-farmer/*srf-3* worm data and the blue curves represent the farmer/wild type worm data. This is on time scales shorter than the reproduction time of the worms. Data for 20 trajectores is shown. **C.** Fraction of worms by genotype that have moved off the patch of bacteria. 20 independent experiments, totaling ∼2000 worms.

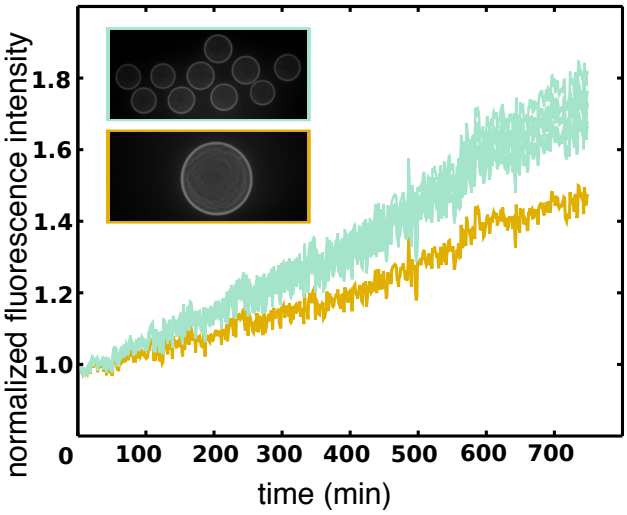

Figure S2: Bacteria distributed in smaller patches grow faster than when compared to the same experiment with one big patch.

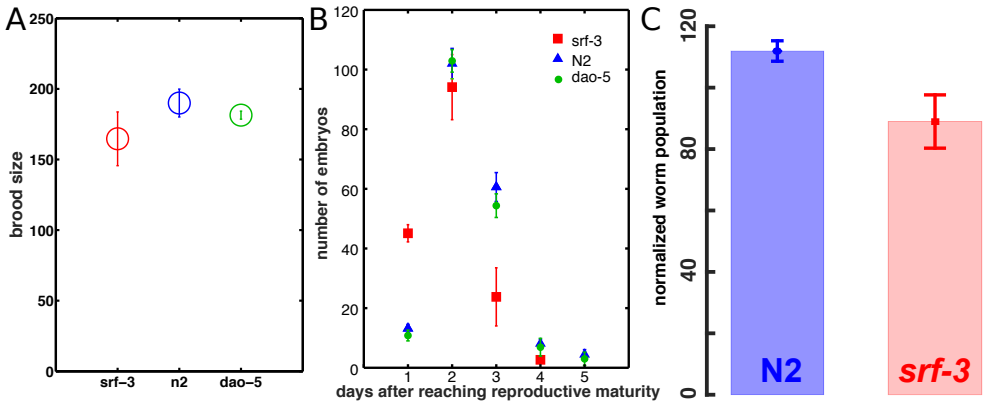

Figure S3: **A**. Mean brood size (progeny per worm life time) for each genotype ($n = 10$ for each genotype). These measurements were made in a controlled setting where farming was inhibited by covering the entire plate with a uniform bacterial lawn. **B**. Eggs laid over time for each genotype. **C** Worm population sizes as shown in main text **Fig. 2C** normalized by respective brood size.

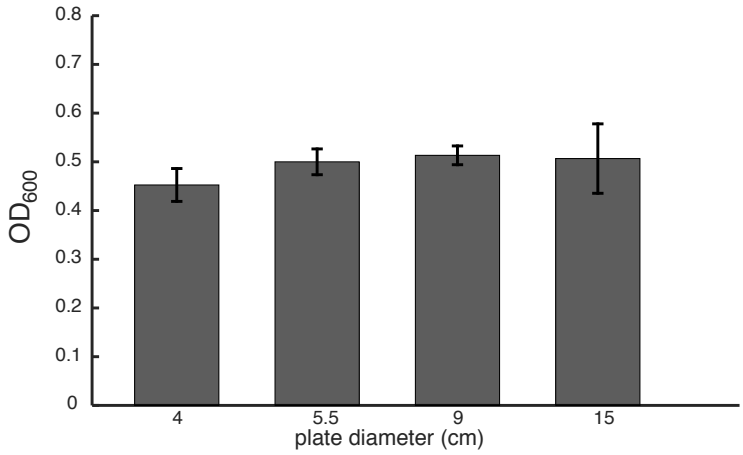

Figure S4: Bacterial growth on petri dishes of different sizes. Optical density (OD_{600}) of bacteria washed off after 48 hours from plates of different diameters with the same initial bacterial seed ($n = 4$ for each time point).

2 Theoretical modeling

We develop a spatially implicit model of *C. elegans* and their bacterial farming behavior. Because very little is known about the worm spatial behavior and the wide gamut of exploitation-exploration strategies employed, the model encapsulates these ideas phenomenologically based on physically- and experimentally-grounded assumptions. Therefore, we do not expect quantitative agreement with the data; rather we aim for qualitative agreement in the context of a simple enough, but physically and biologically-grounded, model that can allow us to test our proposed farming mechanism but also to explore different scenarios and make testable predictions.

Bacteria. Because the feeding and farming behaviors of the worms will be assumed (see below) to affect the area and density of bacteria in ways that can not be captured by the total number of bacteria alone, our model describes the bacteria in terms of its area A_B and density, ρ, instead of using only the total number, B. Of course, the number is determined by these quantities as $B = \rho A_B$. The bacterial growth dynamics in the absence of worms is given by

$$\frac{dA_B}{dt} = g_A A_B \left(1 - \frac{A_B}{\pi R^2}\right), \tag{S.1}$$

$$\frac{d\rho}{dt} = g_\rho \rho \left(1 - \frac{\rho}{K_\rho}\right). \tag{S.2}$$

Here R is the plate radius. The logistic growth captures the experimentally observed behavior that less-dense patches grow faster than dense patches. Parameters g_A, g_ρ and K_ρ are fitted to experimental measurements of the bacterial growth (see Table S1).

Worms. Worms feed on bacteria to grow and reproduce. The worm feeding rate is dependent on the number of bacteria available, the spatial distribution of the bacteria (characterized here by A_B) and the total plate area, πR^2. For simplicity of notation we will write it as $F(A_B, \rho, R)$ to denote that it depends on bacterial and plate characteristics. We describe it via a Holling's type II function, which is a natural ecological assumption

$$F(A_B, \rho, R) = \frac{c\,\Psi\left(A_B, R\right)\rho A_B}{1 + c\,\Psi\left(A_B, R\right)\rho A_B}, \tag{S.3}$$

with a modified attack/encounter rate

$$\Psi(A_B, R) = \exp\left(-\frac{\pi R^2}{\sigma A_B}\right). \tag{S.4}$$

The parameter c controls the rate of increase of the feeding rate with the amount of bacteria available. Our choice of $\Psi\left(A_B, R\right)$ is phenomenological but could be experimentally fitted from the analysis of worm movement. Under the assumption that the encounter rate decreases with large plate size or low available bacteria, we choose $\Psi\left(A_B, R\right)$ to be the modified Gaussian function above. The parameter σ controls how quickly (and at what plate radius

relative to bacterial area) the worm-bacteria encounter rate drops off as the plate radius increases.

Although this constitutes a reasonable choice in the absence of additional mechanistic information on worm space-use, it is important to note that this choice will make quantitative agreement between theory and data unlikely. For instance, on large plates it is likely that memory plays a role in restricting the movement of the worms from the bacteria-rich center of the plate, so that the encounter might not decrease as quickly at large plate sizes as this functional form suggests. Similarly, at early times, the spatial distribution of the initial worm and its progeny on the plate are likely to matter: while it may be true that the encounter rate decreases with plate size for an average worm hatching at some random position on the plate, this is likely untrue for the first worm that is placed initially in the bacteria-rich center of the plate. In turn, the progeny of this first worm may be laid close to the central bacteria patch and also experience a non-average encounter rate. While at longer times over the course of the experiment these spatial correlations may become muted (as eggs are laid further from the center of the plate), our spatially implicit model will fail to capture these early time spatial effects, which could cause quantitative though as we will show not qualitative differences between the theoretical and experimental long time behavior of the near-exponentially growing worm population.

Effect of worms on bacteria: Feeding. The number of bacteria decrease proportional to the worm feeding rate; however, we need to make some assumptions about how the worm feeding may affect the spatial distribution and density of the bacteria. We assume that the area is preserved, but the density is decreased. Essentially this assumes that the bacteria maintains some of the spatial distribution from its growth phase, but becomes ever more diffuse or 'patchy'.

Effect of worms on bacteria: Farming. We expect that the farming behavior will increase the area of the bacteria, decrease the density, but preserve the total amount of bacteria. We introduce a spreading function and we assume that the rate of spreading is proportional to the encounter rate $\Psi(A_B, R)$, and to the amount of free space on the plate (spreading the bacteria is impossible if there is no free space); furthermore, we assume that it increases linearly with the density of the bacteria (worms are less likely to pick up bacteria when it is thinly spread). For simplicity of notation we denote this function by $S(A_B, \rho, R)$ to show its dependence on bacterial and plate characteristics:

$$S(A_B, \rho, R) = s\,\psi(A_B, R)\,\rho\left(\pi R^2 - A_B\right)\,, \tag{S.5}$$

where s is a constant (see Table S1).

2.1 Spatially-implicit model

Based on the discussion above, a model able to capture the worm-bacteria dynamics will have at least three variables, two accounting for the area and density of bacteria and one

accounting for the worms. The worms, W, reproduce at a rate proportional to the feeding rate $F(A_B, \rho, R)$, Eq. (S.3), with a conversion factor ϵ. The model then becomes:

$$\begin{aligned}
\frac{dA_B}{dt} &= g_A A_B \left(1 - \frac{A_B}{\pi R^2}\right) + \frac{A_B}{\rho} S(A_B, \rho, R) W \,, \\
\frac{d\rho}{dt} &= g_\rho \rho \left(1 - \frac{\rho}{K_\rho}\right) - \frac{a}{A_B} F(A_B, \rho, R) W - S(A_B, \rho, R) W \,, \qquad \text{(S.6)} \\
\frac{dW}{dt} &= \epsilon F(A_B, \rho, R) W \,. \qquad \text{(S.7)}
\end{aligned}$$

The parameter s is zero for non-farming srf-3 and greater than zero for farming N2 worms.

Parameter estimation. This spatially-implicit model has eight parameters. The parameters associated with the bacterial growth in the absence of worms, g_A, g_ρ and K_ρ, can be fitted experimentally. This leaves five parameters associated with the worm: a, ϵ, c, σ and s. Three of these, c, σ and s are parameters related to the phenomenological feeding rate $F(A_B, \rho, R)$, and the spreading rate, and they are difficult to fit experimentally. The remaining two parameters a and ϵ do not have unambiguous, measurable analogues in the experimental system. For instance the maximum feeding rate parameter, a, represents the maximum rate at which bacteria is converted into the class 'worms'; however, experimentally, this worm class includes *C. elegans* eggs that neither eat nor reproduce, *C. elegans* juveniles that consume bacteria but do not reproduce, and *C. elegans* adults that both consume bacteria and reproduce. It is therefore not possible to determine a suitable choice for a that appropriately weights each of these life stages, especially when the system is far from equilibrium.

Qualitative agreement with data. Thus, although this version of the model is minimal in terms of the number of variables, it has the downside that most parameters can not be experimentally-inferred. Nevertheless, it can be useful to explore the parameter space and determine (i) the ability of this model and its underlying assumptions to qualitatively capture the experimental observations, and (ii) the robustness of that qualitative agreement. Using this model, we study the dynamics of the farmer, N2 and non-farmer, srf-3 phenotypes independently. We assume that the two types have identical foraging behavior but differ in their ability to spread bacteria. Therefore, we pick c and σ to be the same for both phenotypes but let s be zero for non-farmers and non-zero for farmers. This captures the two types used in our experiments. We allow the five free parameters a, ϵ, c, σ and s to vary and scan parameter space to identify parameters that yield a qualitative agreement between theory and experiment (see Supplementary Movie 5). A reasonable qualitative agreement with experimental data can be found for a broad range of parameter values, as illustrated in Figure S5. In this figure, the parameters have been chosen to illustrate the qualitative agreement between theory and experiment; furthermore, since the worm count is measured experimentally at the time of collapse of the bacterial population on the smallest plate ($t = 144$ hours on the $R = 2$ cm plate), model parameters have also been chosen in such a way that the model results give a similar time of collapse (see Figure S5, lower panel).

Quantitative fit. However, as expected, we note the poor quantitative agreement: this

model overestimates the number of worms in the population by a factor 40. We also note that while it predicts that larger N2 plates do experience enhanced bacterial growth, the model under-predicts the magnitude of this enhancement when compared to that measured experimentally. Although we expected that a spatially-implicit model that only phenomenologically captures details of worm space-use can not give a quantitative fit, there is an additional reason for the large overestimate, a reason which also underlies the inability to fit most of the parameters of this model: the model contains a single worm class, in which the worms are always reproductively capable and produce more reproductively capable worms. This misses the fact that worms lay eggs that take time to hatch and produce sexually immature worms; the latter take time to mature and be able to reproduce; eventually, they become infertile. There are behavioral differences between these age classes that warrant individual descriptions of their dynamics: eggs do not move, consume resources or reproduce; sexually immature worms move, consume resources but do not reproduce; sexually mature worms engage in all behaviors; infertile worms have ceased to reproduce. With one worm class, parameters that reflect reproduction, movement or feeding are necessarily taken to be time averages of the combined population and can not quantitatively capture its dynamics.

2.2 Age-structured spatially-implicit model

In this section we retain the simplicity of the previous model but add age structure to more accurately capture the worm dynamics; this is the full model discussed in the main text. Here we have four worm classes: eggs, W_E, sexually immature worms, W_I, sexually mature worms, W_M, and infertile worms, W_D. The distinct nature of these life stages makes it easier to obtain, directly or from existing literature, experimental estimates on the transition rates between the life stages, for instance the time it takes for an egg to hatch, or the maximum rate at which a juvenile worm can reach sexual maturity (see Table S1).

In the age-structured model, eggs hatch at a constant rate $1/\tau_{hatch}$. Immature, mature and infertile worms all feed. Immature worms do not lay eggs but mature at a rate that depends on their food intake, with a conversion factor ϵ_1. Sexually mature worms lay eggs at a rate that depends on their food intake, with a conversion factor ϵ_2. Sexually mature worms additionally become infertile at a rate proportional to their food intake (and therefore the number of eggs they have laid) with a conversion factor d. Finally, we assume that for the farming N2 worms, only sexually mature and infertile worms are large enough to contribute to the spreading of bacteria.

Overall, the dynamics of the system is described by the following set of ODEs:

$$\begin{aligned}
\frac{dA_B}{dt} &= g_A A_B \left(1 - \frac{A_B}{\pi R^2}\right) + \frac{A_B}{\rho} S(A_B, \rho, R)(W_M + W_D)\,, \\
\frac{d\rho}{dt} &= g_\rho \rho \left(1 - \frac{\rho}{K_\rho}\right) - \frac{a}{A_B} F(A_B, \rho, R)(W_I + W_M + W_D) - S(A_B, \rho, R)(W_M + W_D)\,, \\
\frac{dW_E}{dt} &= \epsilon_1 F(A_B, \rho, R) W_M - \frac{1}{\tau_{hatch}} W_E\,, \\
\frac{dW_I}{dt} &= \frac{1}{\tau_{hatch}} W_E - \epsilon_2 F(A_B, \rho, R) W_I\,, \\
\frac{dW_M}{dt} &= \epsilon_2 F(A_B, \rho, R) W_I - d F(A_B, \rho, R) W_M\,, \\
\frac{dW_D}{dt} &= d F(A_B, \rho, R) W_M\,.
\end{aligned} \tag{S.8}$$

Parameter estimation. We obtained experimental estimates for the majority of our parameters (see Table S1), such that the only free parameters are those related to the phenomenological feeding rate, c, σ and the spreading rate, s. Thus, although the previous version of the model was simpler in the sense that it had the minimal number of variables needed to capture the bacteria-worm interaction, this age-structured version has a much smaller number of free parameters.

Qualitative agreement with data. Using this age-structured spatially-implicit model, we study, as before, the dynamics of the farmer, N2 and non-farmer, srf-3 phenotypes independently. We assume that the two types have identical foraging behavior but differ in their ability to spread bacteria. Therefore, we pick c and σ to be the same for both phenotypes but let s be zero for non-farmers and some positive value for farmers. This captures the two types used in our experiments. We find very good qualitative agreement with the experimental results (Figure S7). We note that the worm numbers resulting from the ODEs have been rescaled (here by a factor of 4) for easier qualitative comparison with the experimental results. The robustness of these results to varying the free parameters in the model is explored in Supplementary Movie 3. Figure S6 further shows the good qualitative agreement in worm number; however it also captures the dependence of the result on the time at which the worm numbers are counted. In the experiments, the worm count was recorded at $t = 144$ hours, the time at which the bacterial population collapsed on the smallest plate ($R = 2$cm) for both N2 and srf-3 worms. In order to align the model results more easily with those obtained experimentally, we have chosen parameters that give the same time of collapse of the bacterial population (see Figure S6). As parameters are varied in the model, this time of collapse will also change. The effect of varying the free parameters on the bacterial dynamics is demonstrated in Supplementary Movie 4. Figure S8 shows how the maximum amount of bacteria across infinite times changes with plate size and worm type. Farming significantly increases the amount of bacteria available.

Quantitative fit. Promisingly, the age-structured spatially-implicit model also provides a quantitative improvement on the previous version of the spatially-implicit model, being

only a factor 4 larger than the experimental values for absolute worm number (see Figures 3 and S7), compared to the factor 40 difference found previously (see Figure S5). It is important to note, however, that even with this extended version of the model, there are still experimental parameters that do not cleanly map onto our theoretical parameters. For instance, our experiments indicate that there are phenotypic differences in the time at which eggs are laid between the srf-3 and N2 worms (see Figure S3): although N2 lay more eggs in absolute terms, srf-3 lay their eggs more rapidly. These differences in number versus speed can not be accounted for with our single egg-laying rate parameter, ϵ_2; this could be solved by including additional worm classes (e.g. sexually mature on day 1, sexually mature on day 2 etc.) but that would further complicate the model without significant additional advantage (while it could lead to an even better quantitative fit, we never expect that fit to be perfect due to the phenomenological aspects). We therefore made a concession to simplicity and decided to approximate ϵ_2 for both genotypes to be equal to their joint average egg-laying rate. Similarly, other parameters, such as feeding rate, egg-laying rate and bacteria spreading rate are likely to vary continuously across worm development. Our model, with only four distinct life stages, does not account for this, primarily because we lack data on how these changes in worm behavior vary continuously with development. Since due to the phenomenological nature of the fitting rate we do not expect quantitative agreement anyway, such an increase in model complexity to reflect a more continuous development is unwarranted since it would not yield a significant quantitative improvement and it would be riddled with parameters that are hard to estimate. Therefore, we henceforth work with the full model above, which has a very small number of free parameters and is sufficiently simple to be useful.

2.2.1 Competition between farmers and non-farmers: same foraging behavior and no additional cost of farming; Figures S9 and S10

In this section we use the age-structured spatially-implicit model to study the dynamics of a mixed system with both farmers and non-farmers competing for the same resource, the bacteria. As above, we assume the the farmers and non-farmers have the same behavior and differ only in their ability to farm (i.e. their stickiness). This setup mirrors our experimental competition setup and the analysis in this section is meant to test whether the assumption that farming is a public good can explain the observed experimental behavior. The ODE

system becomes:

$$
\begin{aligned}
\frac{dA_B}{dt} &= g_A A_B\left(1-\frac{A_B}{\pi R^2}\right)+\frac{A_B}{\rho}S(B,R)\left(W_M^{(N2)}+W_D^{(N2)}\right),\\
\frac{d\rho}{dt} &= g_\rho\rho\left(1-\frac{\rho}{K_\rho}\right)-\frac{a}{A_B}F(A_B,\rho,R)\left(W_I^{(srf3)}+W_M^{(srf3)}+W_D^{(srf3)}+W_I^{(N2)}+W_M^{(N2)}+W_D^{(N2)}\right)\\
&\quad -S(B,R)\left(W_M^{(N2)}+W_D^{(N2)}\right),\\
\frac{dW_E^{(srf3)}}{dt} &= \epsilon_1 F(A_B,\rho,R)W_M^{(srf3)}-\frac{1}{\tau_{hatch}}W_E^{(srf3)},\\
\frac{dW_I^{(srf3)}}{dt} &= \frac{1}{\tau_{hatch}}W_E^{(srf3)}-\epsilon_2 F(A_B,\rho,R)W_I^{(srf3)},\\
\frac{dW_M^{(srf3)}}{dt} &= \epsilon_2 F(A_B,\rho,R)W_I^{(srf3)}-dF(A_B,\rho,R)W_M^{(srf3)},\\
\frac{dW_D^{srf3}}{dt} &= dF(A_B,\rho,R)W_M^{srf3},\\
\frac{dW_E^{(N2)}}{dt} &= \epsilon_1 F(A_B,\rho,R)W_M^{(N2)}-\frac{1}{\tau_{hatch}}W_E^{(N2)},\\
\frac{dW_I^{(N2)}}{dt} &= \frac{1}{\tau_{hatch}}W_E^{(N2)}-\epsilon_2 F(B,R)W_I^{(N2)},\\
\frac{dW_M^{(N2)}}{dt} &= \epsilon_2 F(A_B,\rho,R)W_I^{(N2)}-dF(A_B,\rho,R)W_M^{(N2)},\\
\frac{dW_D^{N2}}{dt} &= dF(A_B,\rho,R)W_M^{N2}.
\end{aligned}
$$

The ratio of the final number of srf-3 and N2 worms, as a function of the initial fraction of the two phenotypes, is plotted in Figure S10. While the general linear trend of the experimental results is captured, the precise slope is not (see Figure 4A). This is in part because the model does not capture the experimental result that on small plates the farming N2 worms exist as smaller numbers on the $R = 2.75cm$ plates than the non-farming srf-3 worms. Consequently, the increase in the number of N2 worms between the $R = 2.75cm$ and $R = 7.5cm$ plates is less in the model than that observed experimentally, resulting in the decreased slope in Figure S10.

2.3 Theoretical explorations and new predictions

Here we use the age-structured spatially-implicit model developed in Section 2 to investigate the system dynamics under several scenarios and make predictions for future experimental work.

2.3.1 Competition between farmers and non-farmers – same foraging behavior but mortality cost for farmers due to pathogenic bacteria; Figure S11

The N2 phenotype, by virtue of its ridged skin, is more susceptible to picking up bacteria, including pathogenic types that are likely to kill it. We propose that this might constitute an indirect cost associated with farming. In order to investigate this idea, we add an additional rate of death to N2 worms in the population. The 'infection' of N2 worms with pathogenic bacteria occurs when food that the worm has trapped around its face/body begins to form a biofilm around the worm's face, suffocating it. We might therefore expect the rate of 'infection' to be proportional to both the bacterial encounter rate and bacterial density. With this is mind, we introduce a death rate due to pathogenic bacteria $\delta\psi(A_B, R)\rho$. The competition equations are the same as in the previous section, except those for the farmer worms which are now modified to account for the extra mortality:

$$\begin{aligned}
\frac{dW_I^{(N2)}}{dt} &= \frac{1}{\tau_{hatch}} W_E^{(N2)} - \epsilon_2 F(A_B, \rho, R) W_I^{(N2)} - \delta\psi(A_B, R)\rho W_I^{(N2)}\,, \\
\frac{dW_M^{(N2)}}{dt} &= \epsilon_2 F(A_B, \rho, R) W_I^{(N2)} - dF(A_B, \rho, R) W_M^{(N2)} - \delta\psi(A_B, R)\rho W_M^{(N2)}\,, \\
\frac{dW_D^{(N2)}}{dt} &= dF(A_B, \rho, R) W_M^{(N2)} - \delta\psi(A_B, R)\rho W_D^{(N2)}\,,
\end{aligned}$$

We find that the increased mortality affects the farmer population negatively and creates an advantage for the non-farmers who can take advantage of the farming without incurring the mortality cost. One additional point worth noting is that the death-by-pathogen rate lowers the effective growth rate of the N2 worm population. In turn, this lowers the rate of increase of the population. During this time, the bacteria has the opportunity to grow to greater abundances. Thus the pathogenic death rate of N2 worms can, in isolation, actually result in an increased overall number of worms relative to the case of no pathogenic death for the N2s. When N2 competes with srf-3, the slowed N2 growth does not result in additional bacterial growth, since this is simply consumed by the srf-3 (see Figure S11).

2.3.2 Competition between two farmers – different foraging behaviors; Figure S12 and S13

In this spatially implicit model, it is difficult to capture explicitly the dynamics of different foraging strategies. However, we can capture this implicitly. The encounter rate $\psi(A_B, R)$ measures how effective the worms are at foraging: a low σ means that the encounter rate decreases rapidly with the amount of empty space on the plate and could be interpreted as an inefficient search strategy, or even a poor memory resulting in the worms getting lost often; a high σ indicates a very good search strategy, or a good memory (the encounter rate is not affected by plate size because the worms find bacteria quickly either due to efficient foraging or due to good memory). In addition to σ, the egg-laying rate ϵ_1 can be used as a proxy for a cost to improved foraging. A worm with a reduced ϵ_1 reproduces more slowly than its counterpart in the presence of the same amount of bacteria. A high σ, low ϵ_1 worm then

forages very efficiently, (space does not affect its feeding rate) but responds to what it does find less efficiently. Arguably this could be interpreted as the metabolic cost paid for more time spent foraging around the plate rather than staying in one location and consuming the bacteria there. Here we investigate what can happen if we vary σ and ϵ_1.

We consider two worms denoted 1 and 2 and for $i = 1, 2$ we write:

$$F^{(i)}(A_B, \rho, R) = \frac{c\,\Psi^{(i)}(A_B, R)\,A_B\rho}{1 + c\,\Psi^{(i)}(A_B, R)\,A_B\rho}\,, \qquad \Psi^{(i)}(A_B, R) = \exp\left(-\frac{\pi R^2}{\sigma_i A_B}\right)\,, \tag{S.9}$$

and

$$S^{(i)}(A_B, \rho, R) = s\,\rho\left(\pi R^2 - A_B\right)\Psi^{(i)}(A_B, R) \tag{S.10}$$

The modified competition equations take the form:

$$\begin{aligned}
\frac{dA_B}{dt} &= g_A A_B\left(1 - \frac{A_B}{\pi R^2}\right) + \frac{A_B}{\rho}\left(S^{(1)}(B,R)W_M^{(1)} + S^{(2)}(B,R)W_M^{(2)}\right)\,,\\
\frac{d\rho}{dt} &= g_\rho\rho\left(1 - \frac{\rho}{K_\rho}\right) - \frac{a}{A_B}\left[F^{(1)}(B,R)\left(W_I^{(1)} + W_M^{(1)}\right) + F^{(2)}(B,R)\left(W_I^{(2)} + W_M^{(2)}\right)\right]\\
&- \left[S^{(1)}(B,R)W_M^{(1)} + S^{(2)}(B,R)W_M^{(2)}\right]\,,\\
\frac{dW_E^{(1)}}{dt} &= \epsilon_1^{(1)}F^{(1)}(B,R)W_M^{(1)} - \frac{1}{\tau_{hatch}}W_E^{(1)}\,,\\
\frac{dW_I^{(1)}}{dt} &= \frac{1}{\tau_{hatch}}W_E^{(1)} - \epsilon_2 F^{(1)}(B,R)W_I^{(1)}\,,\\
\frac{dW_M^{(1)}}{dt} &= \epsilon_2 F^{(1)}(B,R)W_I^{(1)} - dF^{(1)}(A_B,\rho,R)W_M^{(1)}\,,\\
\frac{dW_D^{(1)}}{dt} &= dF^{(1)}(A_B,\rho,R)W_M^{(1)}\,,\\
\frac{dW_E^{(2)}}{dt} &= \epsilon_1^{(2)}F^{(2)}(B,R)W_M^{(2)} - \frac{1}{\tau_{hatch}}W_E^{(2)}\,,\\
\frac{dW_I^{(2)}}{dt} &= \frac{1}{\tau_{hatch}}W_E^{(2)} - \epsilon_2 F^{(2)}(B,R)W_I^{(2)}\,,\\
\frac{dW_M^{(2)}}{dt} &= \epsilon_2 F^{(2)}(B,R)W_I^{(2)} - dF^{(2)}(A_B,\rho,R)W_M^{(2)}\,,\\
\frac{dW_D^{(2)}}{dt} &= dF^{(2)}(A_B,\rho,R)W_M^{(2)}\,.
\end{aligned}$$

In what follows worm 2 will be our $N2$ farmer above such that $\epsilon_1^{(2)} = \epsilon_1$ and $\sigma^{(2)} = \sigma$, with ϵ_1 and σ as in the previous sections. Parameters $\epsilon^{(1)}$ and $\sigma^{(1)}$ pertaining to a hypothetical worm $N1$ will be varied. In Figure S12 and S13 we plot the results of the simulation, for a case in which improved foraging incurs a cost, and a case where it does not.

In this scenario, we find that the benefits accrued from improved foraging are strongly

dependent on plate size. The form of the encounter rate, Eq. (S.9), together with the typical values for $\sigma^{(2)}$ (which we infer from experimental observation, see Table S1), mean that the benefits of improved foraging are muted on small plates and become more prominent as plate size is increased. This can be physically interpreted as implying that distinct foraging strategies lead to encounter rates that differ little on small plates and differ more significantly as the amount of free space on the plate is increased (see Figures S12 and S13).

If the cost to N1 of improved foraging is too high, it is possible for N1 worms to be out-competed (see Figure S12), while if the cost of foraging is small or non-existent, the N1 can out-compete N2 (see Figure S13). In Section 2.3.1, we discussed the counter-intuitive observation that in homogeneous monocultures costs to phenotypes can be beneficial at the population level by releasing pressure on the food resource (bacteria). Similar results hold here (see right panel of Figure S12 and all panels in Figure S13). However, it must be noted that the general observation that "worms that fare worse in competition are comparatively better in isolation" does not always hold; in Figure S12, left panel, the cost of foraging to the N1 worm's reproduction is sufficiently high, and the benefits from foraging sufficiently muted on the small plate, that N1 worms are slightly inferior to N2 worms both in competition and isolation.

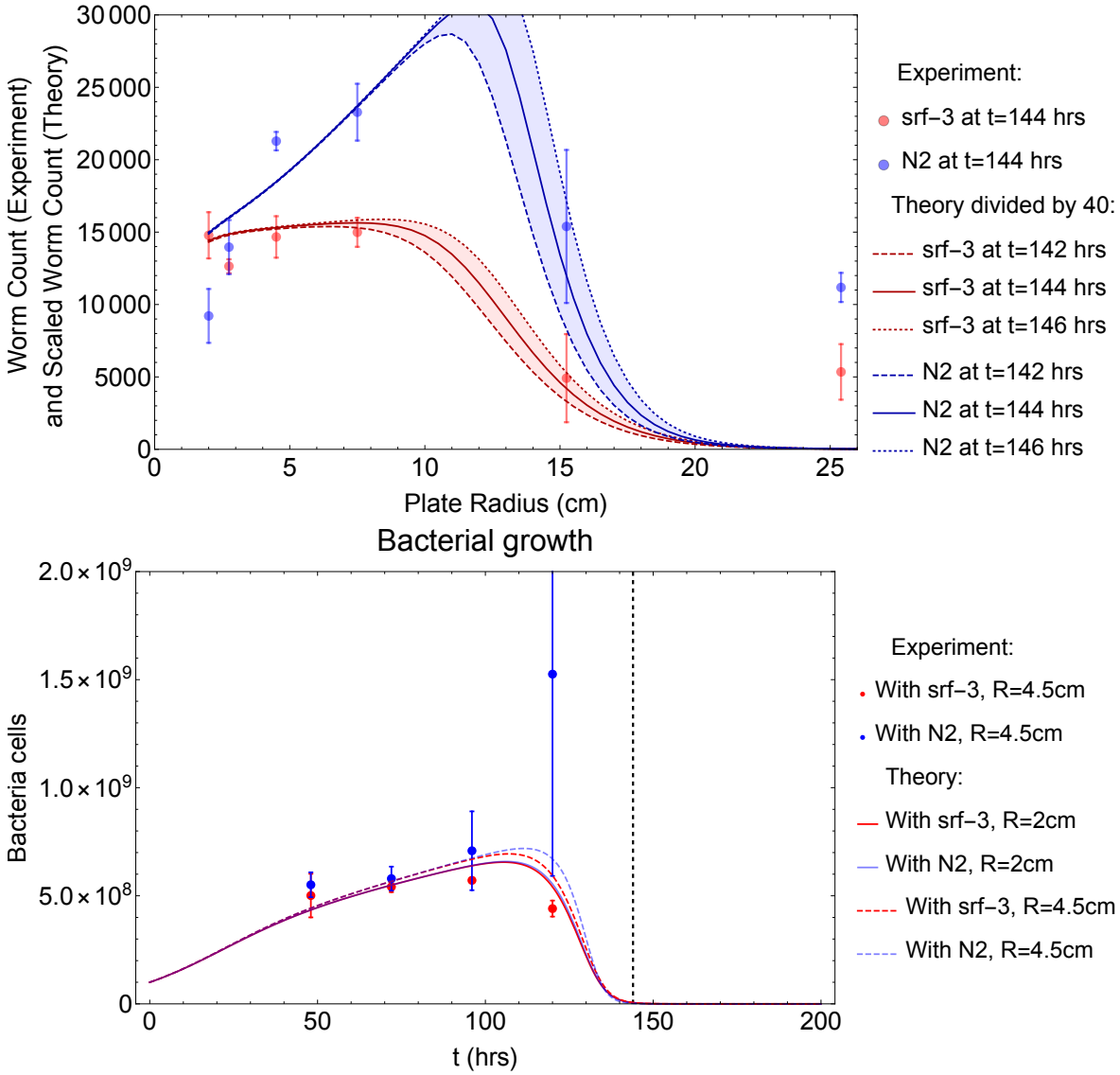

Figure S5: Results from the non-age-structured spatially-implicit model (see Section 2.1). Top panel: Worm count at $t = 144$ hrs as a function of plate size in the model. Dashed lines enclose worm counts at $t = 144 \pm 2$ hrs. Bottom panel: Experimental measurements (markers) and theoretical curves (solid lines) for the bacterial growth on the smallest plate, $R = 2\,\text{cm}$. For both panels, red plots are associated with non-farming srf-3 worms, and blue plots with farming N2 worms. Bacterial growth parameters (g_A, g_ρ and K_ρ) are taken from Table S1. Remaining parameters used are $a = 8$ cells/min, $\epsilon = 4.5 \times 10^{-3}$ min^{-1}, $c = 1.4 \times 10^{-9}$ cells^{-1}, $\sigma = 1200$ cm^2 and $s = 1 \times 10^{-10}$ min^{-1}cm^{-2}. The ODE results for the worm number are divided by 40 for comparison with experimental results. Similar plots are presented in Supplementary Movie 5, where each of the parameters is varied over a range of values.

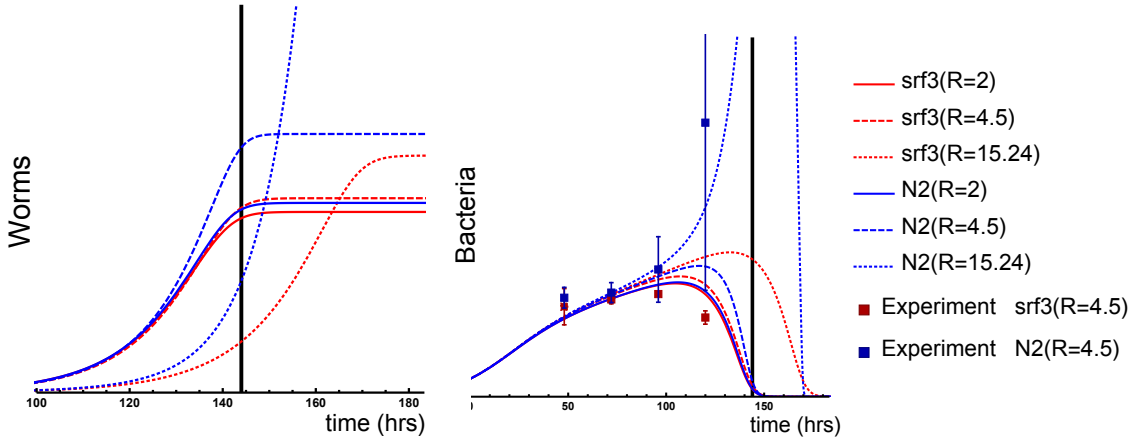

Figure S6: Individual behavior of farmers versus non-farmers in the age-structured spatially-implicit model. Total number of worms ($W_E + W_I + W_M + W_D$) and number of bacteria ($B = A_B\rho$) from the model, shown as a function of time. Parameters taken from Table S1, while s is 0 for non-farming srf-3. Blue curves represent plates with farmers (N2); red curves represent plates with non-farmers (srf-3). The black vertical line represents the time point at which the worm numbers are counted in experiments. Initial conditions: $W_E(0) = W_I(0) = 0$, $W_M(0) = 1$ and $W_D = 0$ for both worms. Overall, farming increases worm number: at shorter time scales (such as the time used for experimental measurements), worms do better on intermediate sized plates because on large plates they do not encounter bacteria as regularly; however, on longer time scales, the bigger the plate, the larger the worm population. This gives good qualitative agreement with the experiments and shows the importance of the time at which worm numbers are compared. The model results show the trajectories that could not be measured experimentally.

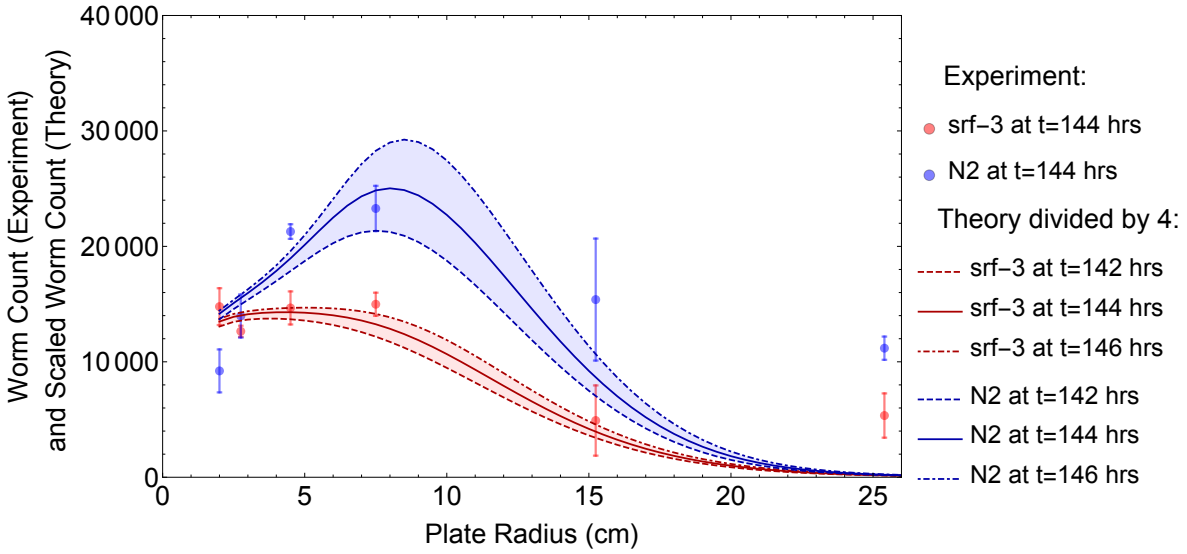

Figure S7: Worm count as a function of plate size in the age-structured, spatially implicit model. Parameters are given in Table S1. Worms are identical in all respects except farming. ODE results divided by 4 to facilitate visual qualitative comparison with experimental results.

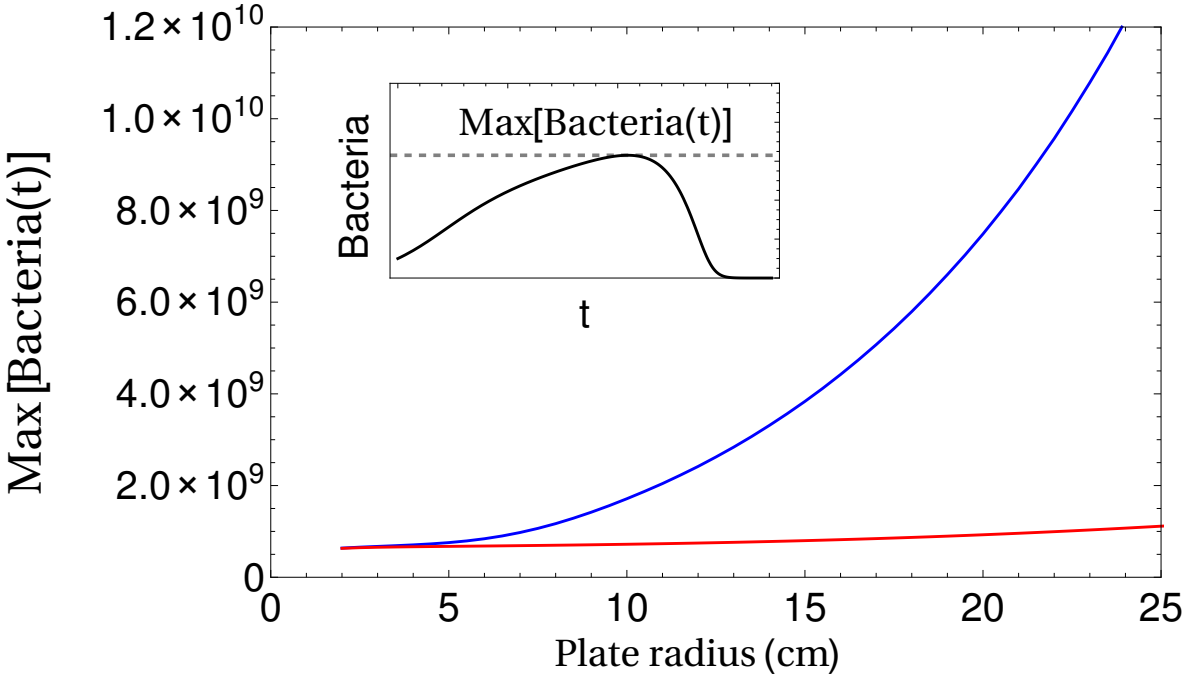

Figure S8: Results of the age-structured spatially-implicit model showing the maximum amount of bacteria present on a plate at any time as a function of plate radius. Plates with srf-3 worm populations are plotted in red: A slight increase in the maximum amount of bacteria is observed as plate size increases, as the bacteria-worm encounter rate is diminished on larger plates, leading to a lower bacteria consumption rate at short times. Plates with N2 worm populations are plotted in blue: The act of farming creates a much larger increase in the maximum amount of bacteria observed as a function of plate size.

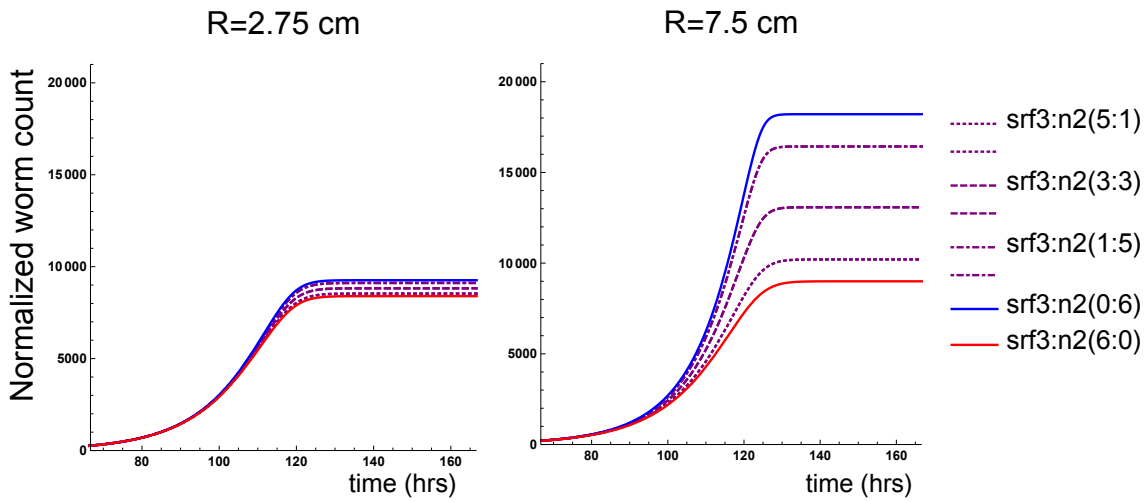

Figure S9: In the absence of fitness costs associated with farming, both worm phenotypes use the public good equally. Worm counts for each phenotype, normalized by the initial worm number of the respective phenotype. Blue = only N2, red = only srf-3, starting with $W_E(0) = W_I(0) = 0$, $W_M(0) = 6$ and $W_D(0) = 0$. Purple curves = mixtures of srf-3 and N2; when normalized by the initial condition, the two worms have identical growth rates. Overall, srf-3 uses the public good to boost its numbers; the more producers there are in the population, the better srf-3 fares. In mixed populations, N2 fares worse than in isolation; the more srf-3 there are, the lower the final total population number. Left panels: plate of size $R = 2.75$ cm; right panels = plate of size $R = 7.5$ cm.

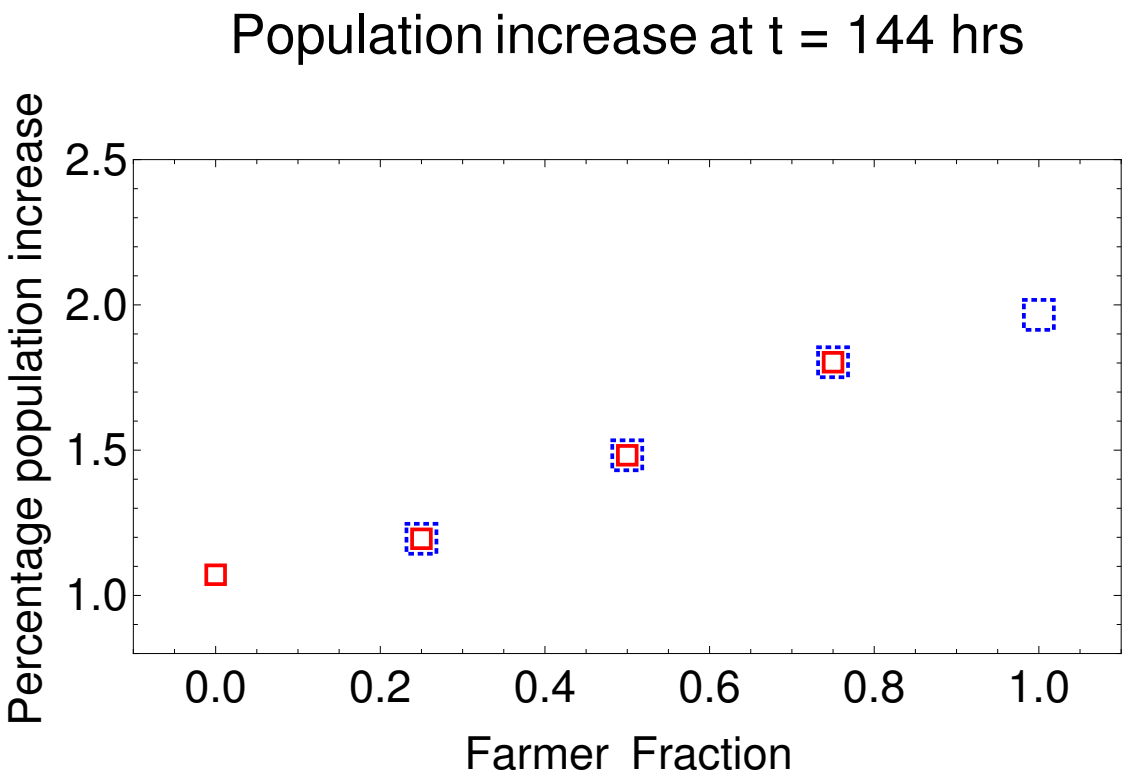

Figure S10: Red (blue) squares = ratio between srf-3 (N2) worm count on a plate of size $R = 7.5$ versus a plate of size $R = 2.75$, taken at time $t = 144$ to allow comparison with the experiments. Measurements are taken under various initial ratios of srf-3 and N2 corresponding to the curves in Figure S9: 6 SRF-3 worms and 0 N2; 5 SRF-3 worms and 1 N2; 3 SRF-3 and 3 N2; 1 SRF-3 and 5 N2; and finally 0 SRF-3 and 6 N2.

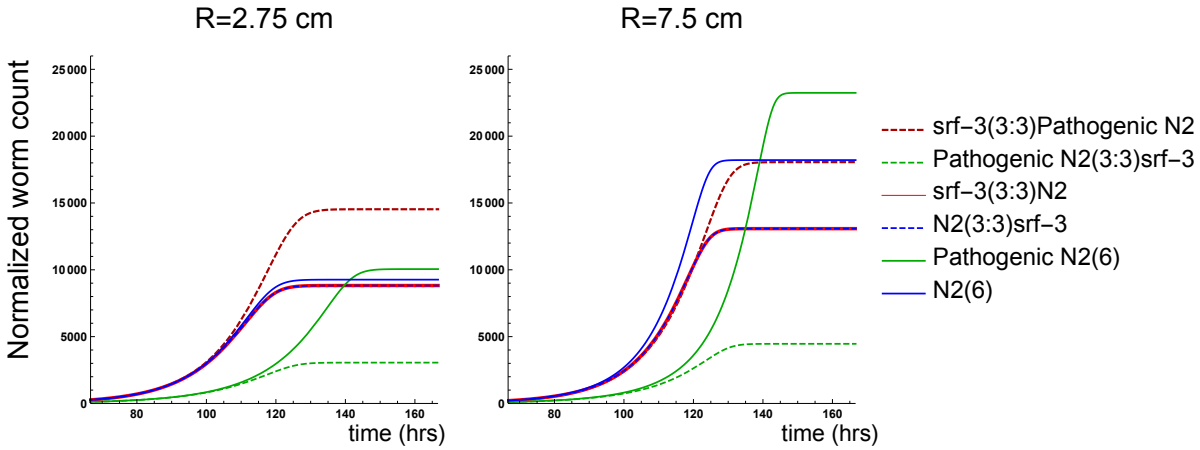

Figure S11: Increased mortality associated with farming behavior leads to the farmer being out-competed by non-farmer (thin dashed dark red curve versus dashed green curve), by comparison to the no-pathogen case where the two phenotypes have identical fitness (the overlapping dashed blue curve and thick dashed red curve). However, in isolation, populations of farmers with increased mortality (green solid curve) fare better than populations of farmers with no mortality cost associated to farming (blue solid curve). This is because individual mortality results in reduced predation pressure on the bacteria which can grow better and ultimately support a larger population of worms. Thus, increased mortality (e.g. due to feeding on pathogenic bacteria) is not something to be avoided if the worms are most likely to interact with their own kind. Left panel = plate size $R = 2.5cm$; right panel = plate size $R = 7.5cm$. Overall, larger plates allow for more farming, which leads to farmers in isolation (blue and green solid curves) reaching larger abundances than the exploiting non-farmers (red curves). Parameters are once again taken from Table S1.

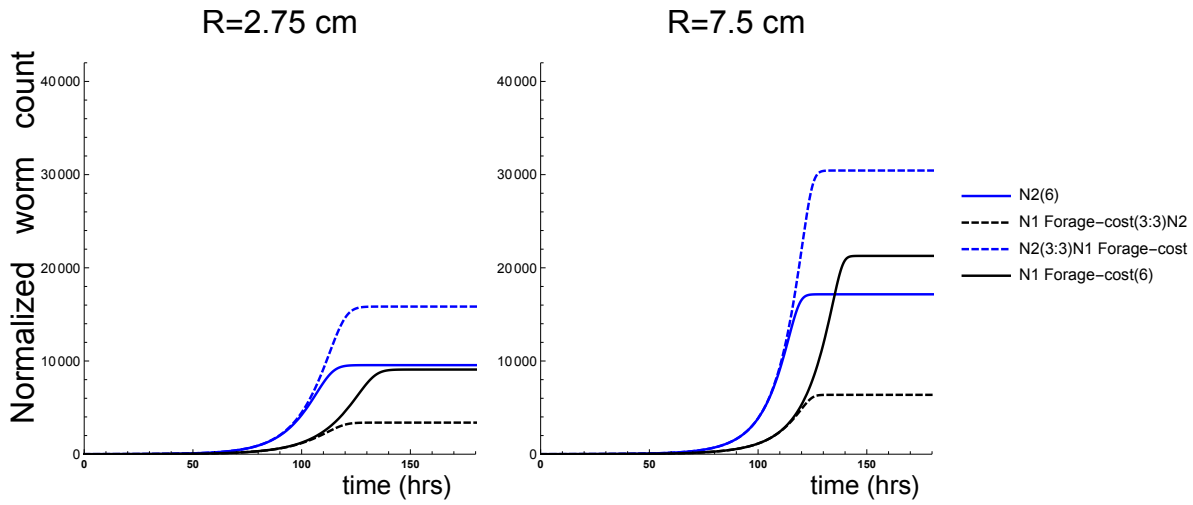

Figure S12: Worm counts normalized by initial worm numbers of each phenotype. Phenotype $N1$ is a more efficient forager than $N2$ ($\sigma^{(1)} > \sigma^{(2)}$) but pays a metabolic cost reflected by a lower egg-laying rate ($\epsilon_1^{(2)} > \epsilon_1^{(1)}$) due to the energetic demands of its foraging. We show two different plate sizes. Blue curves = $N2$; black curves = $N1$. The better forager who simultaneously incurs a cost fares worse (dashed black) than the poorer forager (dashed blue). In isolation however, the better forager who plays a cost (solid black) can fare better due to the reduced pressure it places on the bacterial population. These effects are more likely to be seen as plate size increases because only big enough plates show significant differences between the two foraging strategies – on small plates both $N1$ and $N2$ are similarly good foragers.

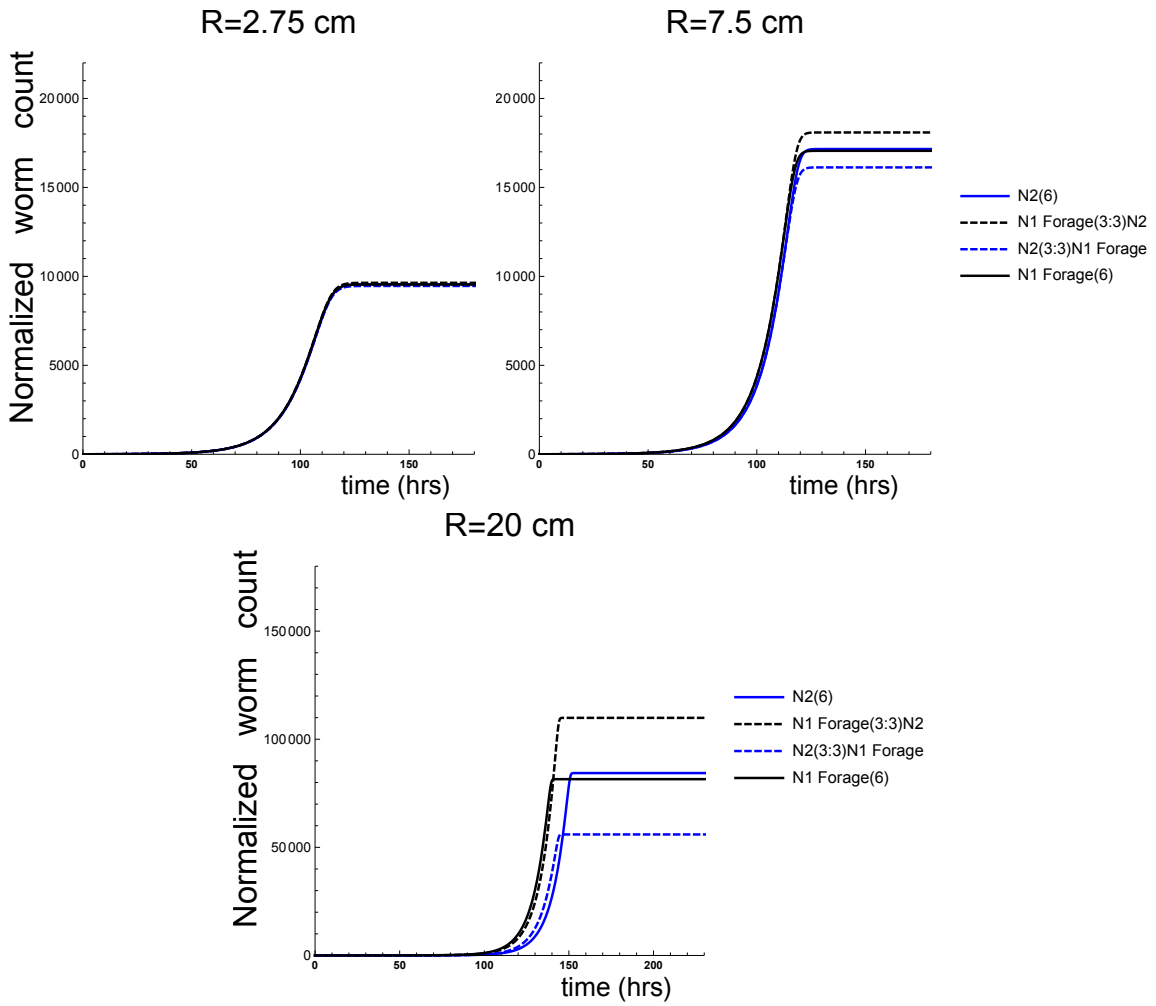

Figure S13: Worm counts normalized by initial worm numbers of each phenotype. Phenotype $N1$ is a more efficient forager than $N2$ ($\sigma^{(1)} > \sigma^{(2)}$) and pays no metabolic cost for this behavior ($\epsilon_1^{(2)} = \epsilon_1^{(1)}$). We show three different plate sizes. As in Figure S12, blue curves = $N2$; black curves = $N1$. The better forager out-competes the other phenotype (dashed black compared to dashed blue), however the effect is exacerbated on larger plate sizes. Once again, the form of the encounter rate, Eq. (S.9), is such that for small plates both $N1$ and $N2$ are similarly good foragers. In isolation, the better foraging $N1$ worm reaches slightly lower numbers than the $N2$ worm, in a manner reminiscent of Figure S12; it forages too well initially, placing an increased pressure on the bacteria, ultimately resulting in a smaller population. However the effect is very minor for small plate sizes.

Tables

Param.	Units	Value	Justification
g_A g_ρ K_ρ	min^{-1} min^{-1} cells/cm^2	1.13×10^{-4} 1.07×10^{-3} 4.58×10^{8}	These parameters are derived from fitting Eqs. (S1) and (S2) to the data in Figure S2. In the fitting it is assumed that florescence intensity is directly proportional to the number of cells. The mapping from cell number to florescence intensity is determined from the initial number of cells on the plate, $N_B(0)$ (see below).
K_A	cm^2	$[\pi 2^2, \pi 25^2]$	The bacteria area carrying capacity is equal to the area of the plate.
a	cells/min	70	Worms have been identified as eating around 70 cells per minute [1].
$\epsilon_1/\epsilon_1^{(2)}$	min^{-1}	3.08×10^{-2}	Experimental results indicated that N2 and srf-3 lay a joint average of 44 embryos per day for 4 days (see Figure S3b).
τ_{hatch}	min	540	Eggs take approximately 9 hours to hatch [2].
ϵ_2	min^{-1}	2.98×10^{-4}	Yields 56 hour mature time. This is the approximate mature time given in literature [2].
d	min^{-1}	1.74×10^{-4}	Worms reproduce for approximately 4 days (see Figure S3b).
δ	$\text{cells}^{-1}\,\text{cm}^2\,\text{min}^{-1}$	8×10^{-13}	Illustrative parameter for exploring model behavior and potential experimental outcomes. Used in Figure S11.
$\epsilon_1^{(1)}$	min^{-1}	$(\epsilon_1^{(2)}/1.5) = 2.05 \times 10^{-2}$	Illustrative parameter for exploring model behavior and potential experimental outcomes. Used in Figures S12-S13.
$\sigma^{(1)}$	cm^2	$1.5 \times \sigma^{(2)} = 1400$	Illustrative parameter for exploring model behavior and potential experimental outcomes. Used in Figures S12-S13.
$N_B(0)$	cells	10^8	Initial number of cells plated in experiments .
$A_B(0)$	cm^2	$\pi 0.5^2$	Initial patch size in experiment.
$\rho(0)$	cells/cm^2	1.27×10^{8}	Initial bacterial concentration.
c	cells^{-1}	2.5×10^{-9}	Parameter chosen to illustrate good visual qualitative fit with data in Figure 3 (see Figure S7). Used in Figures S7-S13.
$\sigma/\sigma^{(2)}$	cm^2	1000	Parameter chosen to illustrate good visual qualitative fit with data in Figure 3 (see Figure S7). Used in Figures S7-S13.
s	$\text{min}^{-1}\text{cm}^{-2}$	7×10^{-9}	Parameter chosen to illustrate good visual qualitative fit with data in Figure 3 (see Figure S7). Used in Figures S7-S13.

Table S1: Parameters used throughout document. Free parameters are highlighted in red.

References

[1] R. L. Gomez-Amaro, E. R. Valentine, M. Carretero, S. E. LeBoeuf, S. Rangaraju, C. D. Broaddus, G. M. Solis, J. R. Williamson, and M. Petrascheck, "Measuring food intake and nutrient absorption in caenorhabditis elegans," 200(2):443-54. *Genetics*, 2015.

[2] Z. F. Altun, and D. H. Hall, "Introduction. In WormAtlas", 2009. doi:10.3908/wormatlas.1.1